Magnetic ordering in the layered Cr(II) oxide arsenides $Sr_2CrO_2Cr_2As_2$ and $Ba_2CrO_2Cr_2As_2$

Magnetic Ordering in the Layered Cr(II) Oxide Arsenides $Sr_2CrO_2Cr_2As_2$ and $Ba_2CrO_2Cr_2As_2$

Xiaoyu Xu, Michael A. Jones, Simon J. Cassidy, Pascal Manuel, Fabio Orlandi, Maria Batuk, Joke Hadermann, and Simon J. Clarke*

ABSTRACT: $Sr_2CrO_2Cr_2As_2$ and $Ba_2CrO_2Cr_2As_2$ with Cr^{2+} ions in CrO_2 sheets and in CrAs layers crystallize with the $Sr_2Mn_3Sb_2O_2$ structure (space group $I4/mmm$, $Z = 2$) and lattice parameters $a = 4.00800(2)$ Å, $c = 18.8214(1)$ Å ($Sr_2CrO_2Cr_2As_2$) and $a = 4.05506(2)$ Å, $c = 20.5637(1)$ Å ($Ba_2CrO_2Cr_2As_2$) at room temperature. Powder neutron diffraction reveals checkerboard-type antiferromagnetic ordering of the Cr^{2+} ions in the arsenide layers below T_{N1_Sr}, of 600(10) K ($Sr_2CrO_2Cr_2As_2$) and T_{N1_Ba} 465(5) K ($Ba_2CrO_2Cr_2As_2$) with the moments initially directed perpendicular to the layers in both compounds. Checkerboard-type antiferromagnetic ordering of the Cr^{2+} ions in the oxide layer below 230(5) K for $Ba_2CrO_2Cr_2As_2$ occurs with these moments also perpendicular to the layers, consistent with the orientation preferences of d^4 moments in the two layers. In contrast, below 330(5) K in $Sr_2CrO_2Cr_2As_2$, the oxide layer Cr^{2+} moments are initially oriented in the CrO_2 plane; but on further cooling, these moments rotate to become perpendicular to the CrO_2 planes, while the moments in the arsenide layers rotate by 90° with the moments on the two sublattices remaining orthogonal throughout [behavior recently reported independently by Liu et al. [Liu et al. *Phys. Rev. B* **2018**, *98*, 134416]]. In $Sr_2CrO_2Cr_2As_2$, electron diffraction and high resolution powder X-ray diffraction data show no evidence for a structural distortion that would allow the two Cr^{2+} sublattices to couple, but high resolution neutron powder diffraction data suggest a small incommensurability between the magnetic structure and the crystal structure, which may account for the coupling of the two sublattices and the observed spin reorientation. The saturation values of the Cr^{2+} moments in the CrO_2 layers (3.34(1) μ_B (for $Sr_2CrO_2Cr_2As_2$) and 3.30(1) μ_B (for $Ba_2CrO_2Cr_2As_2$)) are larger than those in the CrAs layers (2.68(1) μ_B for $Sr_2CrO_2Cr_2As_2$ and 2.298(8) μ_B for $Ba_2CrO_2Cr_2As_2$) reflecting greater covalency in the arsenide layers.

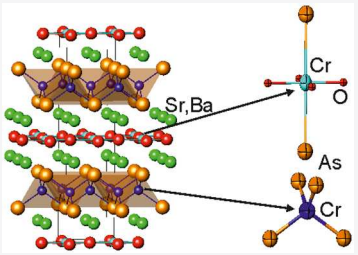

INTRODUCTION

Complex transition metal compounds containing oxide and the anion of a less electronegative element such as a chalcogen (*Ch*: S, Se, Te) or pnictogen (*Pn*: P, As, Sb, Bi) have enjoyed a resurgence since the discovery of high temperature superconductivity in layered iron arsenides and selenides. A common crystal structure adopted by quinary oxide chalcogenides and oxide pnictides is that of the $A_2Mn_3Pn_2O_2$ series (A = Sr, Ba; Pn = As, Sb, Bi) originally reported by Brechtel et al.,[1] extended to include the phosphide $Ba_2Mn_3P_2O_2$[2] and characterized by Brock et al.[3,4] In the structure, A_2MnO_2 layers containing MnO_2 square sheets are separated by anti-PbO-type Mn*Pn* layers with the transition metal ions in edge-shared $MnPn_4$ tetrahedra. This is shown for the title compounds, in which Cr replaces Mn, in Figure 1. The anti-PbO-type pnictide layers are found in superconducting iron arsenides and selenides and in the ZrCuSiAs[5,6] and $ThCr_2Si_2$ or $BaZn_2P_2$ structures.[7,8] Numerous transition metals and Zn may be incorporated into the oxide and chalcogenide or pnictide layers of these oxide chalcogenides and oxide pnictides,[9−11] with the cations of the less electronegative and less oxophilic elements preferentially incorporated into the chalcogenide or pnictide layers.

With two very different transition metal environments in these compounds, the formulas may informatively be written as $A_2MnO_2Mn_2Pn_2$. We adopt this convention for the title compounds $Sr_2CrO_2Cr_2As_2$ and $Ba_2CrO_2Cr_2As_2$ and label the ions as Cr(1) in the oxide layer and Cr(2) in the pnictide layer as in the literature[3,12,13] (Figure 1). The structural relationships between these and related compounds have been reviewed.[14−16]

Compounds with Mn^{2+} ions in both oxide and pnictide layers have been described by Brock et al.[3,4] In $Sr_2MnO_2Mn_2As_2$ and $Sr_2MnO_2Mn_2Sb_2$, moments carried by the Mn ions in the pnictide layers order antiferromagnetically below 340 and 300 K, respectively, with antiferromagnetic coupling of nearest neighbor moments which are directed perpendicular to the layers. A similar magnetic ordering scheme is found for Mn moments in $BaMn_2As_2$ below 625 K[17]

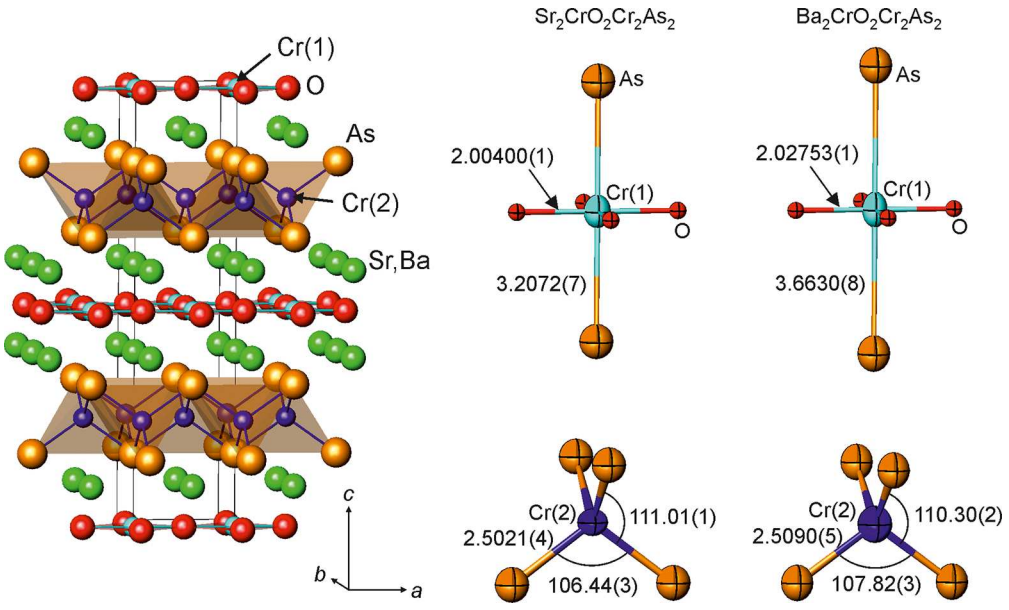

Figure 1. Crystal structure of $Sr_2CrO_2Cr_2As_2$ and $Ba_2CrO_2Cr_2As_2$ with the Cr(1) (oxide layer) and Cr(2) (arsenide layer) sites defined. The details show, to scale, the local coordinations around the Cr(1) and Cr(2) ions in the two compounds. 99% displacement ellipsoids derived from the ambient temperature I11 refinements are shown.

and in *Ln*MnAsO (*Ln* = La, Ce, Nd, Pr) in the regime where only the Mn sublattice is magnetically ordered.[18−20] Brock et al. note the correlation between high ordering temperature and short Mn−Mn distance in the oxide pnictides and related compounds.[4] The manganese moments in the $[MnO_2]^{2-}$ layers of the oxide antimonide $Sr_2MnO_2Mn_2Sb_2$ also show antiferromagnetic coupling of nearest neighbors below 65 K with these moments orthogonal to those in the antimonide layer (i.e., within the MnO_2 plane)[3] and the moments in the two layers behaving as independent magnetic systems.[21] In $Sr_2MnO_2Mn_2As_2$, $Sr_2MnO_2Zn_2As_2$, and $Ba_2MnO_2Zn_2As_2$, only short-range ordering of the MnO_2 layer magnetic moments was observed.[3,11,22] $Sr_2MnO_2Mn_2As_2$,[22] $BaMn_2As_2$,[23,24] and *Ln*MnAsO compounds (*Ln* = early lanthanide)[19,25] with similar MnAs layers are reported to be semiconducting.

Recently Jiang et al.[12] reported the synthesis of the Cr analogue $Sr_2CrO_2Cr_2As_2$ with Cr ions of nominal oxidation state +2 in both the distended octahedral CrO_4As_2 site in the oxide layers (Cr(1)) and in the tetrahedral $CrAs_4$ site (Cr(2)) in the arsenide layers. The compound $Sr_2CrFe_2As_2O_2$ has also been reported recently,[26] although the characterization by X-ray diffraction does not allow the extent of Fe/Cr ordering to be determined in that case. Given the general difficulty of stabilizing the Cr^{2+} oxidation state for Cr in oxides, Jiang et al.[12] entertained the reasonable possibility that in $Sr_2CrO_2Cr_2As_2$ the oxidation state was slightly greater than +2 in the oxide layer and slightly less than +2 in the arsenide layer. They also reported that a small level of contamination by a ferromagnetic chromium arsenide[27] impurity ($T_C \sim 230$ K) was very difficult to avoid and that this hampered the characterization of the intrinsic magnetic susceptibility, although there was evidence from magnetic susceptibility and heat capacity measurements for a magnetic ordering transition at 291 K. Compounds with similar CrAs layers are known, and in LaCrAsO[28] and $BaCr_2As_2$,[29] it is found that, unlike the Mn analogues, the compounds exhibit metallic resistivity but with substantial localized moments on the Cr ions. An antiferromagnetically ordered moment of 1.57 μ_B was found at room temperature in LaCrAsO;[28] $BaCr_2As_2$ was predicted from first-principles calculations[29] to show ordering of localized Cr moments well above room temperature, and it was confirmed that this compound indeed orders antiferromagnetically with $T_N = 580(10)$ K.[30] Jiang et al.[12] found that $Sr_2CrO_2Cr_2As_2$ also exhibits itinerant behavior and predicted that both the Cr(1) and Cr(2) sublattices would exhibit antiferromagnetic ordering using density-functional calculations within the generalized gradient approximation. In a parallel investigation to our own reported here, Liu et al.[13] recently described the temperature dependence of the magnetic ordering behavior of $Sr_2CrO_2Cr_2As_2$ in which two independent Cr^{2+} sublattices ordering magnetically with different propagation vectors are somehow coupled, resulting in a spin-reorientation transition described below. Here we provide evidence from high resolution diffraction investigations for why $Sr_2CrO_2Cr_2As_2$ shows anomalous spin-reorientation behavior. As a contrast, we report additionally the new isostructural Ba analogue, $Ba_2CrO_2Cr_2As_2$, in which the two Cr^{2+} sublattices remain independent. We compare and contrast the behavior with the Mn analogues and related compounds.

EXPERIMENTAL METHODS

Synthesis. $Sr_2CrO_2Cr_2As_2$ was prepared on the 3-g scale by reacting together SrO, Cr (Alfa 99.95%), and As (Alfa 99%) in stoichiometric amounts with the aid of a CsI flux. SrO was made by thermal decomposition of $SrCO_3$ (Alfa 99.994%) under dynamic vacuum (at 830 °C for 16 h followed by 1100 °C for 4 h). Stoichiometric amounts of the starting materials were ground together with an equimolar amount of dry CsI (Alfa 99.998%) (i.e., molar ratio of "$Sr_2Cr_3As_2O_2$":CsI = 1:1) and placed in an alumina crucible of mass ~30 g which was, in turn, placed in an evacuated silica ampule that had been predried under vacuum to avoid hydrolysis of the products by water adsorbed on the surface of the ampule. The ampule was heated to 1100 °C at a ramp rate of 2 °C min^{-1}: the slow ramp rate ensuring that the volatile arsenic reacts before it attains a high vapor pressure, and then the temperature was maintained at 1100 °C for 48 h before the furnace was switched off and the ampule was allowed to cool to room temperature. After cooling, the black powder

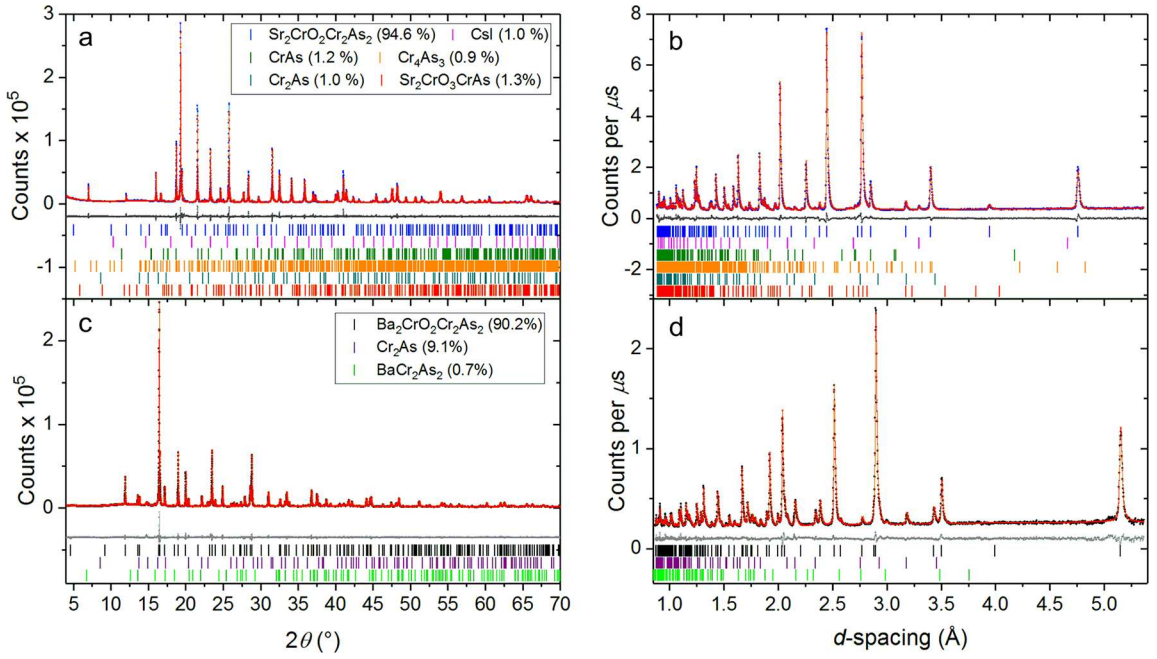

Figure 2. Rietveld refinements of the nuclear structure of $Sr_2CrO_2Cr_2As_2$ against synchrotron PXRD data (I11) collected at room temperature (a) and PND data (WISH) at 623 K (b). (c) and (d) show equivalent Rietveld refinements for $Ba_2CrO_2Cr_2As_2$: synchrotron PXRD data at room temperature (c) and PND data at 473 K(d). Data from the 2θ = 120° data bank of WISH is presented in (b) and (d).

product remained in the alumina crucible, while the CsI flux was found to have mostly evaporated on to the surface of the silica tube. Consequently it was found to exist as a very minor contaminant in the product (~1% by mass), and the samples were analyzed without further attempts at purification, as washing had previously been found to introduce further contamination; the presence of CsI also aided temperature calibration in the PND experiment as described below. The use of the CsI flux reproducibly yielded the purest samples. Attempts to replicate the synthesis presented by Jiang et al.[12] (a flux-free ceramic synthesis at 900 °C from SrO, Cr, and As) generally produced higher levels of contamination, and indeed, the recent work of Liu et al. confirms this.[13] In particular, in our syntheses, a persistent unidentified impurity was found with the most intense reflection at 2.79 Å (subsequently identified using electron microscopy as a new phase of formula $Sr_2Cr_2AsO_3$), although the use of higher firing temperatures of 1100−1200 °C did result in products approaching the purity obtained using the CsI flux. Because of the air-sensitivity of some of the reagents and possible air-sensitivity of the product, all manipulations and storage of the samples were carried out in an argon-filled glovebox. The characterization was carried out on two 3-g samples (referred to as sample 1 and sample 2 in what follows). A polycrystalline sample of $Ba_2CrO_2Cr_2As_2$ was prepared by a solid-state reaction using BaO (Aldrich 99.99%), Cr (Alfa 99.95%), and As (Alfa 99%) as starting materials in stoichiometric amounts. A pellet of the ground mixtures of the starting materials was placed in an Al_2O_3 crucible which was then sealed inside an evacuated predried silica ampule. First, the sample was heated to 800 °C for 24 h at a slow rate of 2 °C/min, so that the As was reacted completely before it reached a high vapor pressure in the tube (the boiling point of As is 613 °C).[1] The mixture was then reground for homogenization, pressed into a pellet, heated to 1200 °C at 10 °C min^{-1}, and sintered at this temperature for 4 h followed by quenching into ice/water.

Diffraction Measurements. Powder X-ray Diffraction (PXRD) measurements were performed using the instrument I11 at the Diamond Light Source Ltd., UK with 0.826 Å X-rays (calibrated using a Si standard before each series of experiments).[31] High resolution diffraction patterns were collected on both samples at ambient temperature and at 100 K for $Sr_2CrO_2Cr_2As_2$ using the multianalyzer crystal (MAC) detector of this instrument. Variable temperature PXRD patterns for $Sr_2CrO_2Cr_2As_2$ were obtained every 24 s using the MYTHEN position sensitive detector (PSD). Three such measurements were made: on cooling in a nitrogen cryostream between 290 and 100 K at a rate of 6 K min^{-1}, on warming in the cryostream between 250 and 400 at 6 K min^{-1}, and on warming using a hot air blower between 300 and 673 at 6 K min^{-1}. Powder Neutron Diffraction (PND) measurements were performed on both compounds using the WISH diffractometer[32] at the ISIS Facility, UK. For $Sr_2CrO_2Cr_2As_2$, samples 1 and 2 were contained inside 6 mm diameter vanadium cylinders. Sample 2 was measured only at ambient temperature, and sample 1 was measured in the temperature range 1.5 K − 320 K in a helium cryostat and separately in the range from room temperature to 623 K in a resistance furnace. Cadmium metal was used to mask the steel part of the sample container below room temperature, while gadolinium foil was used for the same purpose above RT. For $Ba_2CrO_2Cr_2As_2$, the sample was contained in a 6 mm vanadium cylinder with a gadolinium foil mask and measured in a closed cycle refrigerator equipped with a heating stage insert that enabled measurements on warming from ambient temperature to 600 K, followed by measurement on cooling to 5.5 K. Rietveld refinements of the crystal and magnetic structures and model-independent Pawley-type fits against powder diffraction data were carried out using Topas Academic Version 5.[33] The web-based software ISODISTORT[34] was used to aid the deduction of the magnetic models prior to Rietveld refinement.

Transmission Electron Microscopy. Electron diffraction (ED) patterns on $Sr_2CrO_2Cr_2As_2$ (sample 1) were acquired on a Philips CM20 transmission electron microscope operated at 200 kV at room temperature and at ~−170 °C (following *in situ* cooling). High angle annular dark field (HAADF) scanning transmission electron microscopy (STEM) images were acquired using a FEI Titan 80-300 "cubed" microscope operated at 300 kV. A specimen for the TEM study was prepared by grinding the material under ethanol and depositing a few drops of the suspension onto a copper TEM grid covered by a holey carbon layer. The specimen was prepared in air.

Magnetometry. All measurements used a Quantum Design MPMS-XL SQUID magnetometer. For both $Sr_2CrO_2Cr_2As_2$ and $Ba_2CrO_2Cr_2As_2$, the susceptibility was determined by measuring the magnetization as a function of temperature on warming from 2 to 320 K after cooling both in zero applied field (zero-field cooled (ZFC)) and then in the measuring field (field cooled (FC)) of 50 mT

Table 1. Refinement Results for $Sr_2CrO_2Cr_2As_2$ (Sample 1) and $Ba_2CrO_2Cr_2As_2$[a]

compound	$Sr_2CrO_2Cr_2As_2$		$Ba_2CrO_2Cr_2As_2$	
instrument	I11	WISH	I11	WISH
radiation	X-ray	Neutron	X-ray	Neutron
wavelength (Å)	0.825901	white beam	0.82606	white beam
temperature (K)	298	623	298	473
R_{wp} (%)	7.90	3.51	8.05	3.58
space group	*I*4/*mmm*	*I*4/*mmm*	*I*4/*mmm*	*I*4/*mmm*
a (Å)	4.00800(2)	4.03128(7)	4.05506(2)	4.07085(2)
c (Å)	18.8214(1)	19.0399(4)	20.5637(1)	20.5893(2)
V (Å^3)	302.347(4)	309.42(1)	338.140(4)	341.20(4)
ρ (g cm^{-3})	5.63573(8)	5.5069(2)	6.01558(7)	5.96161(8)
Cr(1)−O (Å) [4]	2.00400(1)	2.01564(4)	2.02753(1)	2.03542(0)
Cr(1)−As (Å) [2]	3.2072(7)	3.2391(6)	3.6630(8)	3.6793(9)
Cr(2)−As (Å) [4]	2.5021(4)	2.5251(3)	2.5090(5)	2.5096(5)
Sr/Ba−O (Å) [4]	2.5964(5)	2.6228(4)	2.7351(3)	2.7408(7)
Sr/Ba−As (Å) [4]	3.2333(5)	3.2499(4)	3.4001(5)	3.4184(8)
As−Cr−As (deg) [2]	106.44(3)	105.93(2)	107.82(3)	108.40(4)
As−Cr−As (deg) [4]	111.01(1)	111.27(1)	110.302(15)	110.010(16)

[a]Fits are shown in Figure 2.

($Sr_2CrO_2Cr_2As_2$) or 100 mT ($Ba_2CrO_2Cr_2As_2$). Magnetization isotherms ($-5 \leq \mu_0 H/T \leq 5$) were measured after cooling the sample from 300 K to the measurement temperature in a 5 T field. For these measurements at ambient temperature or below, samples of about 30 mg in mass were contained in gelatin capsules. Further measurements on both $Sr_2CrO_2Cr_2As_2$ and $Ba_2CrO_2Cr_2As_2$ were made in the range $300 \leq T/K \leq 650$ using the furnace insert for the MPMS-XL magnetometer: the fresh samples were measured on warming (ZFC) and on cooling (FC) in an applied field of 0.5 T. For these measurements, the samples were contained in thin-walled silica ampules.

RESULTS

Synthesis and Crystal Structure Refinement. For $Sr_2CrO_2Cr_2As_2$, the synthesis using the CsI flux route produced the highest quality samples according to the laboratory PXRD patterns. Rietveld analysis of the synchrotron PXRD data taken at ambient temperature and 100 K (Figure 2(a)) and PND data on sample 1 above the temperature where magnetic Bragg peaks are evident (see below) (Figure 2(b)) revealed small amounts of crystalline impurity phases which we have not been able to entirely eliminate, but all peaks were accounted for in the refinements. The diffraction measurements confirmed the model of Jiang et al.,[12] and the refined structural parameters are presented in Table 1. Jiang et al. found that "*nearly single-phase samples could be prepared only by a small deviation of stoichiometry with 2−5% oxygen deficiency*" implying a possible degree of nonstoichiometry; however, we tested this and found no evidence for oxygen deficiency from the synthesis nor from the refinements against PND data and speculate that additional oxygen to compensate for the deficiency introduced by Jiang et al.[12] could arise from the silica tubes. We also found no variation between samples of $Sr_2CrO_2Cr_2As_2$ outside the variation expected from making independent measurements of different samples (see Table 4). $Ba_2CrO_2Cr_2As_2$ was successfully synthesized only when high firing temperatures were used. The sample was contaminated by a significant amount of Cr_2As impurity and some $BaCr_2As_2$, and the diffraction pattern also contained some unindexed reflections which we presume arise from an as-yet unidentified Ba-containing impurity. In this case, also there was no evidence from the refinements for bulk nonstoichiometry in the main phase. The refinement results against ambient temperature synchrotron PXRD data and high temperature (above the magnetic ordering transitions) PND data for sample 1 of $Sr_2CrO_2Cr_2As_2$ and the sample of $Ba_2CrO_2Cr_2As_2$ are given in Tables 1−3 and Figure 2. See also Tables S1−S6 and Figures S3 and S4.

Table 2. Structural Parameters for $Sr_2CrO_2Cr_2As_2$ from Rietveld Refinement against I11 RT Data

atom	site	*x*	*y*	*z*	U_{11},U_{22} (Å^2)[a]	U_{33} (Å^2)
Sr	4e	0	0	0.41229(4)	0.0107(3)	0.0133(5)
Cr(1)	2a	0	0	0	0.0098(5)	0.015(1)
Cr(2)	4d	0	0.5	0.25	0.0126(4)	0.0098(6)
As	4e	0	0	0.17040(4)	0.0155(3)	0.0165(5)
O	4c	0	0.5	0	0.004(1)[b]	0.004(1)[b]

[a]$U_{11} = U_{22}$ by symmetry for sites refined anisotropically. [b]O atoms refined isotropically

Table 3. Structural Parameters for $Ba_2CrO_2Cr_2As_2$ from Rietveld Refinement against I11 RT Data

atom	site	*x*	*y*	*z*	U_{11},U_{22} (Å^2)[a]	U_{33} (Å^2)
Ba	4*e*	0	0	0.41073(2)	0.0149(2)	0.0161(3)
Cr(1)	2*a*	0	0	0	0.0090(6)	0.018(1)
Cr(2)	4*d*	0	0.5	0.25	0.0176(5)	0.0199(8)
As	4*e*	0	0	0.17813(4)	0.0152(4)	0.0189(6)
O	4*c*	0	0.5	0	0.012(2)[b]	0.012(2)[b]

[a]$U_{11} = U_{22}$ by symmetry for sites refined anisotropically. [b]O atoms refined isotropically.

Table 4 shows that there is little evidence, from the lattice and structural parameters, of compositional variation between the samples of $Sr_2CrO_2Cr_2As_2$, which might have arisen from the slight oxygen nonstoichiometry proposed by Jiang et al.[12] Refinement of the fractional oxygen occupancy in $Sr_2CrO_2Cr_2As_2$ using PND data at 623 K produced a refined value of 1.017(3) which we deem to indicate full occupancy, so there was no indication of the possible oxygen deficiency proposed by Jiang et al.[12] Because of the low atomic number of O, the refinements against synchrotron data were relatively

Table 4. Comparison of $Sr_2CrO_2Cr_2As_2$ Samples from Ambient Temperature Synchrotron PXRD Data

sample	a (Å)	c (Å)	c/a	V (Å^3)	z(Sr)	z(As)	χ^2	R_{wp} (%)
Jiang et al.[12]	4.0079(1)	18.8298(3)	4.6982(2)	302.47(1)	0.4123(1)	0.1701(1)	3.0	7.3
sample 1[a]	4.00800(2)	18.8214(1)	4.69596(4)	302.347(4)	0.41229(3)	0.17040(3)	2.22	7.90
sample 2[b]	4.00856(8)	18.8268(4)	4.6967(1)	302.52(1)	0.41251(3)	0.17056(3)	5.37	1.72

[a]MAC detector. [b]MYTHEN PSD detector.

insensitive to the fractional occupancy of the site, and occupancies ranging between 0.92 and 1.08 were obtained depending on whether the form factor for O^{2-} or neutral O respectively was used. In the PND experiment, O makes a relatively larger contribution to the scattering, and the scattering length is independent of the chemistry of the element. A similar analysis for $Ba_2CrO_2Cr_2As_2$ in which Rietveld refinements against both X-ray and neutron powder diffraction data were used to investigate the possibility of deficiencies on the oxide site and the Cr site in the arsenide layer concluded that this compound too was stoichiometric within the experimental uncertainty of 1−2%.

Magnetic Susceptibility. Magnetic susceptibility measurements below room temperature for $Sr_2CrO_2Cr_2As_2$ were similar to those reported by Jiang et al.[12] and were dominated by a small amount of ferromagnetic chromium arsenide impurity which we were not able to eliminate in the syntheses. It is clearly extrinsic to the main phase because the magnetization varied in magnitude from sample to sample. The $Ba_2CrO_2Cr_2As_2$ sample was evidently free from this impurity and showed no signs of magnetic transitions below room temperature (Figure S11(a)). SQUID magnetometry measurements above room temperature (see Figure S11(b) for $Ba_2CrO_2Cr_2As_2$) were noisy on account of the experimental configuration; we found that there were no clear features associated with magnetic ordering in these susceptibility measurements, so we use the analysis of the PND data to discuss the ordering phenomena.

Magnetic Ordering. PND measurements on $Sr_2CrO_2Cr_2As_2$ revealed that there were intense diffraction peaks present at ambient temperature which were not predicted by the structural model although these diminished to the background level on warming the sample above 600(10) K and were most intense at long d-spacings, suggesting that they arose from long-range magnetic ordering. Hence, we report above the nuclear-only crystal structure refinement above from PND data collected at 623 K (Figure 2, Table 1). Measurements below a Néel temperature estimated in our measurements as 600(10) K (similar within the uncertainty to the 590.3(7) K determined by Liu et al.[13]) down to 1.5 K revealed dramatic changes in the relative intensities of these reflections around room temperature as shown in Figure 3(a). Similar measurements on $Ba_2CrO_2Cr_2As_2$ revealed similar sets of magnetic reflections evident in the neutron diffractograms collected below 473(10) K (Figure 3(b)). The quantitative thermal evolution of the reflections in the two compounds are quite different as we discuss below.

Between 598 K and 348 K in $Sr_2CrO_2Cr_2As_2$ and, at lower temperatures, between 473 and 233 K in $Ba_2CrO_2Cr_2As_2$, the magnetic Bragg peaks (peaks marked "+" in Figure 3) were modeled successfully by just introducing long-range ordering of the magnetic moments of the Cr(2) ions in the CrAs layers. Nearest-neighbor moments were coupled antiferromagnetically in a checkerboard fashion with the moments directed along the c-direction perpendicular to the planes in both compounds.

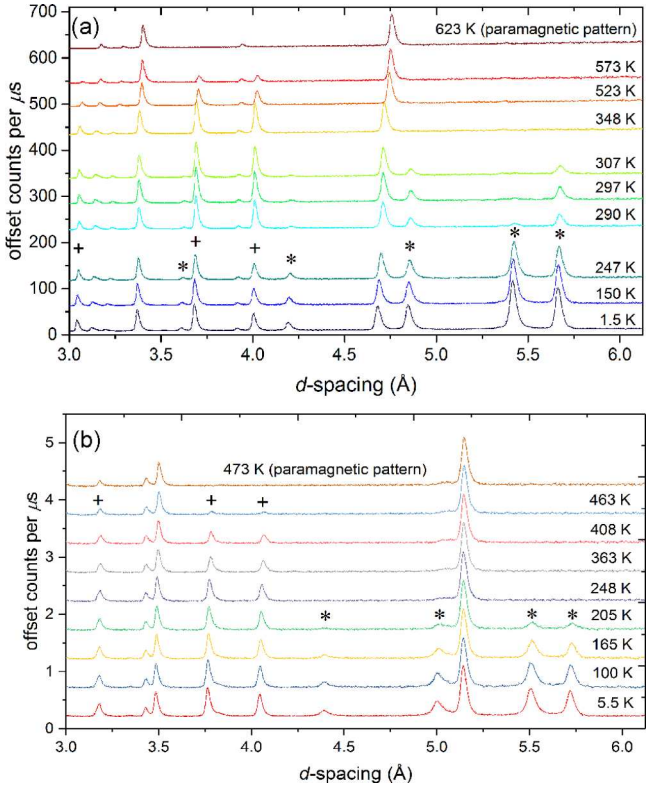

Figure 3. (a) WISH PND data of $Sr_2CrO_2Cr_2As_2$ in the range 1.5 to 623 K (combination of banks 3 and 8 at $2\theta = 90°$). The data have been offset along the vertical axis for clarity. Several magnetic peaks marked with (*) and (+) are present at 1.5 K, which all persist on warming to 247 K. At 290 K, the peaks marked (*) have greatly diminished in intensity and are absent at 348 K. However, the peaks marked (+) increase in intensity over the same range. Above 348 K, the magnetic peaks marked (+) diminish in intensity and are completely absent in the pattern collected at 623 K. The changes in intensity result from the onset of ordering of the moments on the two Cr sublattices occurring at different temperatures and from a spin-reorientation transition as described in the main text. (b) Analogous data for $Ba_2CrO_2Cr_2As_2$ with the magnetic Bragg peaks labeled in a similar way. For a further description of the similarities and differences in the two compounds, see text.

The ordering scheme is similar to that displayed by the Mn analogues with As or Sb pnictide ions[3] and to the compounds LaCrAsO[28] and $BaCr_2As_2$[30] with similar CrAs layers, except that the Cr(2) moments in adjacent layers related by the vector $\mathbf{c}/2$ are aligned parallel in $Sr_2CrO_2Cr_2As_2$ and $Ba_2CrO_2Cr_2As_2$ rather than antiparallel. In this high temperature regime, the moments carried by the Cr(1) ions in the CrO_2 layers were found not to contribute to the magnetic Bragg peaks. Figure 4(a) shows the refinement and the magnetic model for $Sr_2CrO_2Cr_2As_2$ at 348 K after the reflections marked with (+) symbols in Figure 3(a) have grown significantly in intensity. Figure 5(a) shows the refinement at a similar stage for $Ba_2CrO_2Cr_2As_2$. In this high

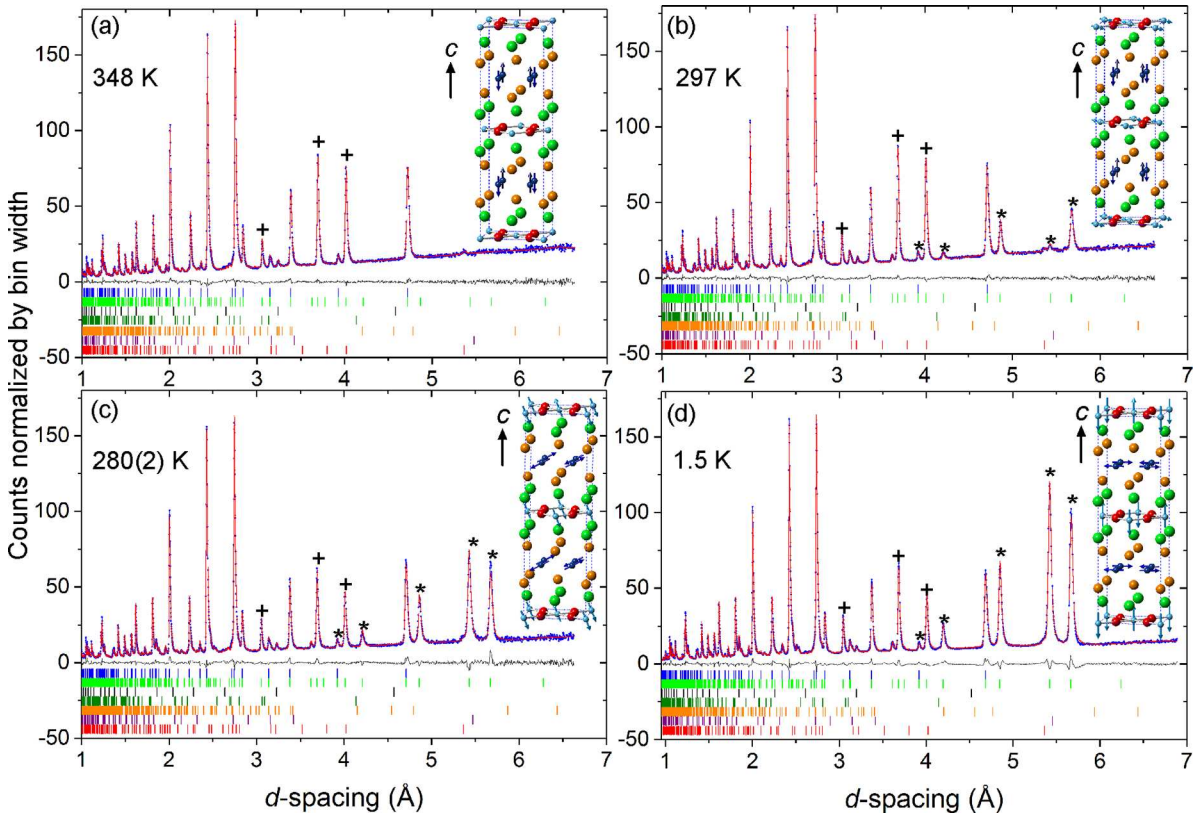

Figure 4. Rietveld refinements against PND data for $Sr_2CrO_2Cr_2As_2$ from WISH bank 3/8 ($2\theta = 90°$). The insets depict the ordering and relative magnitudes and orientations of the magnetic moments at the given temperature. (a) At 348 K, one set of magnetic peaks is observed due to ordering of the Cr(2) sublattice (dark blue), the most prominent of which are labeled with a cross (+). $\chi^2 = 0.75$, $R_{wp} = 3.62$. (b) At 297(1) K, an additional set of magnetic peaks appears due to ordering of the Cr(1) sublattice (light blue), labeled with an asterisk (*). $\chi^2 = 0.79$, $R_{wp} = 3.59$. (c) At 280(2) K, the magnetic peaks have grown and are changing their relative intensity. $\chi^2 = 0.75$, $R_{wp} = 4.07$. (d) At 1.5 K, the magnetic peaks reflect the low temperature ordering regime. $\chi^2 = 0.85$, $R_{wp} = 4.05$. Note the difference in the ratios of magnetic peaks between (b) and (d) resulting from the spin-reorientation. In the plots, the data (blue), fit (red), and difference (gray) are shown. Tickmarks are from the top as follows: $Sr_2CrO_2Cr_2As_2$ nuclear (94.6% by mass), $Sr_2CrO_2Cr_2As_2$ magnetic, CsI (1.2%), CrAs (1.2%), Cr_4As_3 (0.9%), Cr_2As (1.0%), and Sr_2CrO_3CrAs (1.3%). Sr (green), As (orange), and O (red) atoms are also depicted.

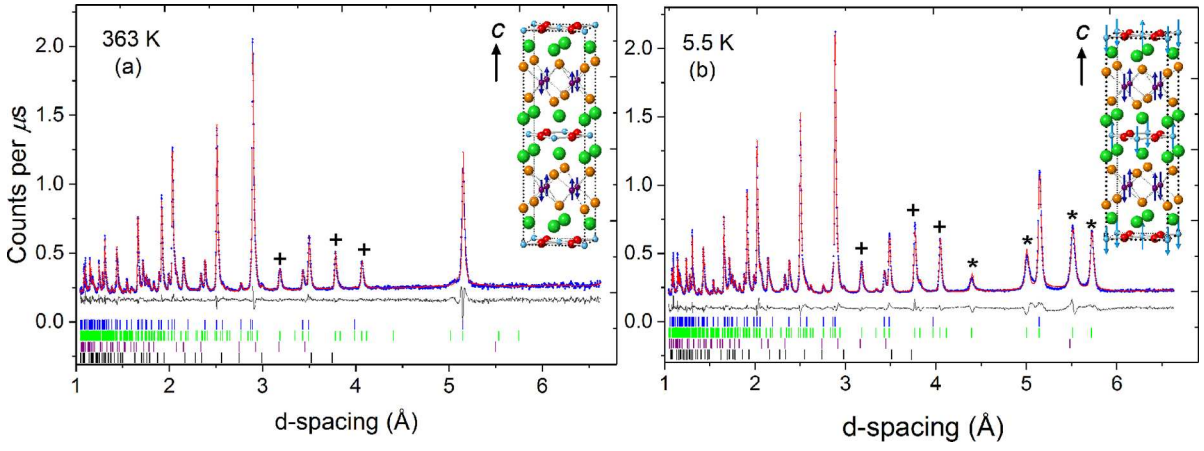

Figure 5. Rietveld refinement against PND data for $Ba_2CrO_2Cr_2As_2$ at (a) 363 K and (b) 5.5 K from WISH bank 3/8 ($2\theta = 90°$). The insets depict the ordering and relative magnitudes of the magnetic moments. Data (blue), fit (red), and difference (gray) are shown. Tickmarks are from the top as follows: $Ba_2CrO_2Cr_2As_2$ nuclear, $Ba_2CrO_2Cr_2As_2$ magnetic, Cr_2As (9.1% by mass), and $BaCr_2As_2$ (0.7%). + indicates magnetic Bragg peaks arising from ordering of the Cr(2) moments (dark blue), and * indicates magnetic Bragg peaks arising from ordering of the Cr(1)moments (light blue). Ba (green), As (orange), and O (red) atoms are also depicted.

temperature regime, the magnetic structure described by the Cr(2) moments has a $k = (1\ 1\ 1)$ propagation vector and can be described using a primitive tetragonal cell with lattice parameters $a_{nucl} \times a_{nucl} \times c_{nucl}/2$ relative to the nuclear cell.

For $Sr_2CrO_2Cr_2As_2$, additional magnetic reflections (those labeled with (*) in Figure 3(a) and Figure 4) became apparent, and these emerge between 325 and 348 K and persist to lower temperatures. Similar reflections emerge in

$Ba_2CrO_2Cr_2As_2$ below 233 K (Figure 3(b) and Figure 5). New magnetic models were deduced for both compounds in which the moments of the Cr(1) ions in the oxide layer participate in long-range order with antiferromagnetic coupling of nearest neighbor moments. For these moments, the propagation vector is $k = (1/2\ 1/2\ 0)$ (requiring a $\sqrt{2}a_{nucl} \times \sqrt{2}a_{nucl} \times c_{nucl}$ magnetic unit cell). However, the details of these magnetic models are different in $Sr_2CrO_2Cr_2As_2$ and $Ba_2CrO_2Cr_2As_2$, and, in particular, the magnetic scattering of $Sr_2CrO_2Cr_2As_2$ shows some anomalies as described below which have not been observed previously.[13] In $Ba_2CrO_2Cr_2As_2$, the fits to the data below 233 K (Figure 5(b)) are consistent with Cr(1) oxide layer moments that are directed, like the Cr(2) arsenide layer moments, parallel to the *c* direction. On cooling, the Cr(1) long-range ordered moment grows in magnitude and becomes larger than the Cr(2) long-range ordered moment below 200 K. At the lowest temperature, both moments in $Ba_2CrO_2Cr_2As_2$ are saturated and are directed parallel to the *c*-axis.

In contrast, just below 348 K in $Sr_2CrO_2Cr_2As_2$ the major component of the Cr(1) moment lies in the *ab*-plane parallel to the CrO_2 layers, with an antiferromagnetic nearest neighbor Cr(1) coupling arrangement similar to that found for the Mn moments in the MnO_2 layers of $Sr_2MnO_2Mn_2Sb_2$[3] but orthogonal to that found at the onset of ordering of these Cr(1) moments in $Ba_2CrO_2Cr_2As_2$. In $Sr_2CrO_2Cr_2As_2$, the magnetic intensities were satisfactorily modeled when these moments were slightly canted toward the *c*-axis direction as shown in Figure 4(b) for the data collected at 297(1) K. Refinement of a canting of the Cr(2) moments toward the *ab*-plane was also attempted. At 297 K, the refined value of the canted component did not deviate from zero, and at 290 K, the value was 0.2(2) μ_B.

In $Sr_2CrO_2Cr_2As_2$, the magnitude of the Cr(1) (oxide layer) ordered moment at 297 K is 1.61(1) μ_B. This increases rapidly on cooling and overtakes the magnitude of the Cr(2) (arsenide layer) moments by 248 K. Between these temperatures, a gradual reorientation of the direction of both sets of moments takes place in $Sr_2CrO_2Cr_2As_2$: the Cr(1) moments in the oxide layer rotate from the *ab*-plane to lie along the *c*-axis, and the Cr(2) moments in the arsenide layer rotate *vice versa*. This behavior of $Sr_2CrO_2Cr_2As_2$ has recently been reported by Liu et al.,[13] and our results are consistent with theirs. We note here that our PND measurements in this reorientation region straddling room temperature were measured on warming in the cryostat which was not optimized for controlling temperature or measuring the sample temperature in this range. It was evident from the comparison of the magnetic scattering intensities of sample 1 inside the cryostat with the magnetic scattering intensities measured for both samples 1 and 2 at room temperature outside the cryostat, that the sample temperature was systematically overestimated by the cryostat thermocouple. So, calibration of the sample temperature was performed using the behavior of the lattice parameters of both the main phase and CsI impurity, and these are the temperatures quoted in the text (see Figure S1 and Table S7).

The spin reorientation is, as suggested by Liu et al.,[13] presumably the origin of the feature in the magnetic susceptibility and the heat capacity noted by Jiang et al.[12] Refinement of the magnetic structure at 280(2) K (Figure 4(c)) shows the majority component of the Cr(1) moments in the oxide layer is now directed along the *c*-axis, and the Cr(2) spins in the arsenide layer are now significantly rotated onto the *ab*-plane, with a larger component of the moment lying in the *ab*-plane than in the *c*-direction. The moments on the Cr(1) and Cr(2) sublattices remain orthogonal.

By 247(1) K, attempted refinement of a remanent *ab*-component in the Cr(1) moment for $Sr_2CrO_2Cr_2As_2$ produced a value of 0.73(2) μ_B, and refinement of a remanent *c*-component for the Cr(2) moment produced a value of 0.77(3) μ_B although the agreement factors were only marginally smaller (>0.05%) than when these minority components were set to zero. So, within the certainty of the measurement, the spin-reorientation transition (SRT) appears to be complete. So at this temperature and below in $Sr_2CrO_2Cr_2As_2$, the Cr(2) moments in the arsenide layer are, within the experimental uncertainty, directed completely within the *ab*-plane, and the Cr(1) moments in the oxide layer are directed purely along the *c*-direction. This arrangement of the moments is observed to persist at all lower temperatures, with the moments on both Cr(1) and Cr(2) sublattices reaching saturation at around 100 K. The refinement at 1.5 K is shown in Figure 4(d). Note that powder neutron diffraction measurements place an intrinsic constraint on knowing the moment orientation in an ordered system.[35] The component along the principal *c*-axis may be determined unambiguously, but the orientation of any component within the *ab*-plane perpendicular to the principal axis is uncertain.

Figure 6(a) summarizes the changes in the magnetic model for $Sr_2CrO_2Cr_2As_2$ with temperature, and Figures 7(a) and 7(b) show the changes in the magnitudes of the refined moments and their components. In contrast, $Ba_2CrO_2Cr_2As_2$ shows no spin-reorientation transition, and both Cr(2) and Cr(1) moments are oriented along the *c* direction (Figures 6(b) and 7(c)).

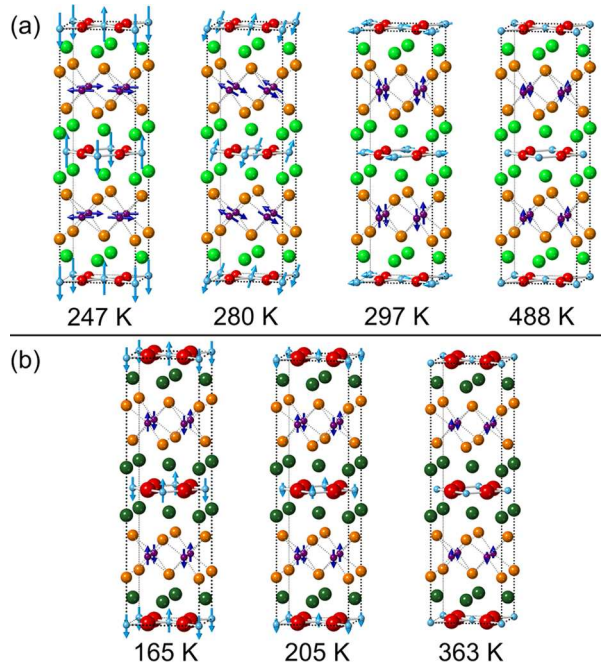

Figure 6. (a) Magnetic unit cell of $Sr_2CrO_2Cr_2As_2$ over the temperature range 1.5−623 K, showing the magnitude and direction of magnetic moments for the two chromium sublattices. (b) Analogous diagrams showing the evolution in $Ba_2CrO_2Cr_2As_2$.

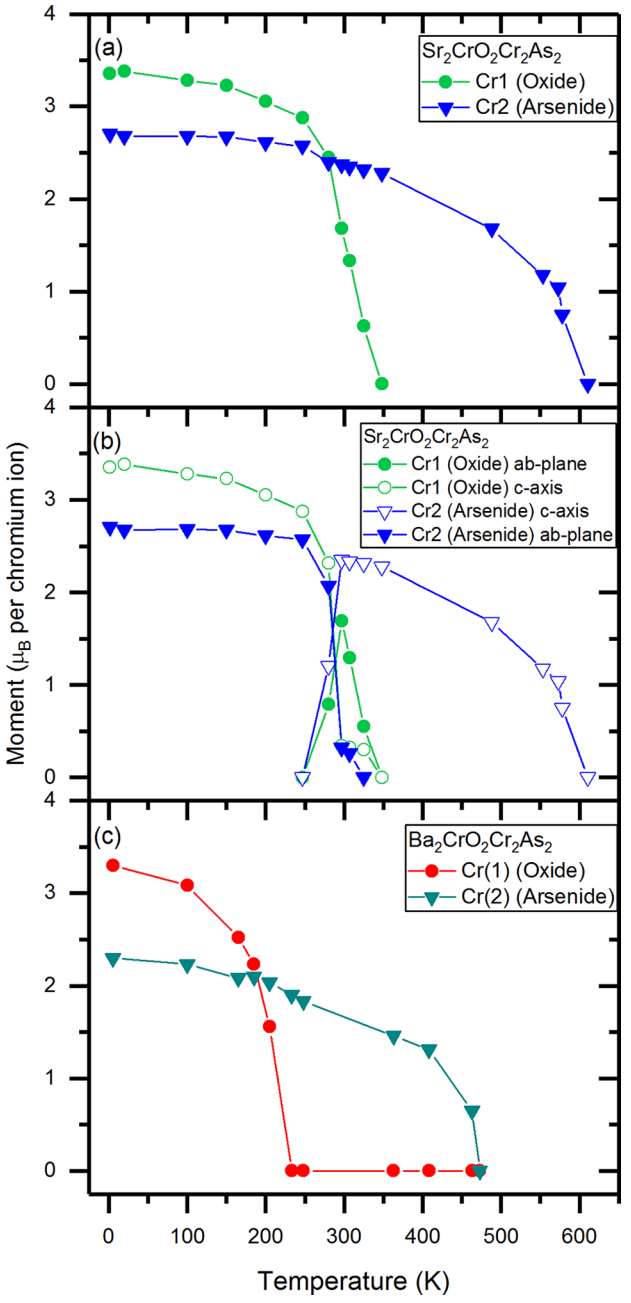

Figure 7. (a) Magnitudes and (b) magnitudes and directions of the long-range ordered moments in the two Cr sublattices of $Sr_2CrO_2Cr_2As_2$ as functions of temperature. (c) Magnitudes of the moments in the two Cr sublattices of $Ba_2CrO_2Cr_2As_2$ as a function of temperature.

The high resolution across a wide *d*-spacing range available on the WISH instrument enabled us to observe clearly two further features of the magnetic scattering in $Sr_2CrO_2Cr_2As_2$ that were not present in $Ba_2CrO_2Cr_2As_2$ and which may be important in explaining why the spin-reorientation transition found by us and by Liu et al.[13] occurs in $Sr_2CrO_2Cr_2As_2$ given that two sublattices ordering with different propagation vectors should not, in principle, couple to one another. These features have not been described previously. First, we observed in the low-angle data bank on WISH the emergence between 280(2) K and 247 K of a further feature in the long *d*-spacing region at about 16.2 Å. This feature, which we presume to be magnetic in origin, because there is no corresponding feature in 100 K X-ray diffraction data (Figure S12), is at a similar *d*-spacing to the intense 0 0 1 reflection of a minor impurity identified as Sr_2CrO_3CrAs with the Sr_2MnO_3CuS structure.[36] However, on further cooling it moves significantly to longer *d*-spacings (it moves much more, and in the opposite direction to that expected for thermal contraction) as shown in Figure 8, reaching 16.8 Å at 1.5 K.

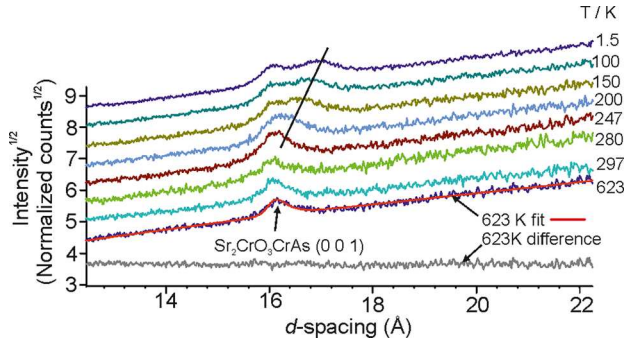

Figure 8. Extra magnetic scattering at long *d*-spacings visible in the low angle (2θ = 27°) data banks on WISH. The intense (0 0 1) nuclear reflection of the Sr_2CrO_3CrAs impurity (1.3% by mass) is fitted against the 623 K data. The extra scattering emerges from a similar *d*-spacing at the temperature of the spin reorientation transition in the main $Sr_2CrO_2Cr_2As_2$ phase and shifts markedly to longer *d*-spacings on further cooling as shown by the guideline. The patterns are offset by 0.6 units along the intensity$^{1/2}$ axis. See Figure S12 for comparative X-ray data showing the lack of this additional scattering.

Second, below 290 K in $Sr_2CrO_2Cr_2As_2$ a slight discrepancy occurs between the locations of the magnetic peaks and the positions predicted on the basis of the tetragonal structural unit cell. The discrepancy is only clearly evident in the fit to the (101/011) and (010/100) reflections for the magnetic unit cell, which lie at *d*-spacings of 5.42 and 5.66 Å, respectively. These are purely magnetic reflections (they correspond to the (1/2 1/2 1) and (1/2 1/2 0) reflections for the nuclear unit cell). From 280 K down to 1.5 K, the discrepancy can be well accounted for by refining the *a* and *b* lattice parameters of the magnetic unit cell independently of one another with the *c* lattice parameter fixed to that of the nuclear unit cell. Model independent (Pawley) fits to the 1.5 K data from WISH banks 3/8 and 5/6 improved from a R_{wp} of 4.24% when the structural and magnetic cells were constrained to be tetragonal with $a_{mag} = \sqrt{2} \times a_{nucl.}$ to R_{wp} = 2.89 when the nuclear cell was constrained to be tetragonal and the magnetic cell was allowed to be orthorhombic. A further slight decrease in R_{wp} to 2.62% was found when the nuclear cell was also allowed to be orthorhombic, thus suggesting a possible small orthorhombic distortion occurring in the structure below 290 K. Figure 9 shows the effect on the long *d*-spacing magnetic reflections of fitting the pattern using a single Pawley (model independent) phase which was either tetragonal (Figure 9(a)) or orthorhombic (Figure 9(b)). Applying this method of modeling to the 100, 150, 200, 250, and 280 K data shows a decrease in the degree of the apparent orthorhombic distortion on warming, accompanied by a convergence of the agreement factors when modeling the magnetic peaks as either tetragonal or orthorhombic (Figure S2 and Table S8). The apparent distortion of the unit cell follows the growth in the magnitude

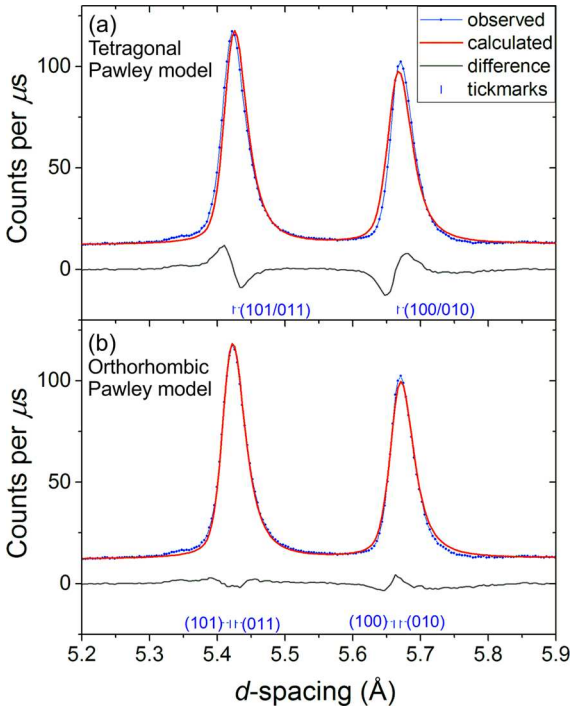

Figure 9. Comparison of the fit when using (a) a tetragonal or (b) an orthorhombic model and refining the unit cell metric and peak intensities independently of the structure (Pawley refinement). Fitting was carried out against all 5 detector banks, including the Pawley refinement of the magnetic peaks only and Rietveld refinement of the nuclear peaks of tetragonal $Sr_2CrO_2Cr_2As_2$ (95.3%), CsI (1.2%), CrAs (1.2%), Cr_4As_3 (1.3%), and Cr_2As (1.0%). The agreement factor R_{wp} for the fit as a whole drops from 4.27% with the tetragonal model to 3.54% with the orthorhombic model. The indices for these purely magnetic reflections refer to the $\sqrt{2}a \times \sqrt{2}a \times c$ expansion of the nuclear cell.

of the component of the Cr(2) moments in the arsenide layer directed in the *ab*-plane (Figure 7(b)) suggesting that it is associated with the spin reorientation. We examined this behavior further by running WISH in "double-frame" mode in which alternate neutron pulses were discarded, allowing the relevant range of *d*-spacings to be probed on a higher resolution detector bank. The behavior was observed to be similar, and we rule out that it is an artifact of the measurement.

We probed whether there really was a symmetry lowering of the crystal structure via exchange-striction by performing measurements of the X-ray diffraction pattern with a higher reciprocal space resolution using the synchrotron powder diffractometer I11 at Diamond and measuring data using the high resolution MAC detector. This showed no evidence of the nuclear unit cell undergoing any distortion between ambient temperature and 100 K (Figure S4), although the reciprocal space resolution is about five times higher on I11 ($\Delta d/d$(FWMH) $\sim 2 \times 10^{-3}$ at $d \sim 2$ Å) than on WISH ($\Delta d/d$(FWMH) $\sim 10^{-2}$). Furthermore, no sharp transitions are evident in the behavior of the lattice parameters or unit cell volume in the range 100 to 673 K, and the behavior is qualitatively similar to that shown by the CsI impurity (Figure S5). Low temperature electron diffraction measurements (Figure S8) also offered no evidence for a structural change. Thus, the slight shift of the purely magnetic peaks in Figure 9(a) from their expected positions is not simply a consequence of a structural distortion.

DISCUSSION AND CONCLUSIONS

Crystal Structures. The structure type accommodates a range of cations and anions. In comparing $Sr_2CrO_2Cr_2As_2$ with the Ba analogue, significant changes in the interatomic distances (Table 1) result from the increase in size of the alkaline earth cation. The *a* lattice parameter and hence the Cr(1)−O and Cr(2)−Cr(2) distances increase by 1.17% on substituting Sr^{2+} for Ba^{2+}. The Cr(2)−As distance in the arsenide layers increases only marginally (0.3%), so the $Cr(2)As_4$ tetrahedra which are slightly compressed in the *ab*-plane become more regular in $Ba_2CrO_2Cr_2As_2$. With the basal plane expansion restricted by maintaining strong Cr(1)−O and Cr(2)−As interactions, the larger Ba^{2+} cation is accommodated disproportionately by expansion of the cell perpendicular to the basal plane, and the *c* lattice parameter increases by 9.3%. Thus, the most significant change in coordination environment for a Cr ion is the 14% increase in the Cr(1)−As distance, from 3.207(1) Å in $Sr_2CrO_2Cr_2As_2$ to 3.663(1) Å in $Ba_2CrO_2Cr_2As_2$ which makes the already highly distended $Cr(1)O_4As_2$ environment even more distended, and in $Ba_2CrO_2Cr_2As_2$, Cr(1) is close to being in a purely square planar CrO_4 coordination environment.

Table 5. Lattice Parameters and Selected Bond Distances for Reported $Sr_2Mn_3As_2O_2$-Type Oxide Arsenides with Different First Row Transition Metals or Zn

variable	comment			
compound	$Sr_2CrO_2Cr_2As_2$	$Sr_2CrO_2Fe_2As_2$	$Sr_2MnO_2Zn_2As_2$	$Sr_2MnO_2Mn_2As_2$
reference	this work	26	11	3
T (K)	298	298	298	300
a (Å)	4.00806(3)	3.9948(1)	4.12624(3)	4.1500(4)
c (Å)	18.8216(2)	18.447(1)	18.6709(2)	18.867(2)
c/*a*	4.6959(1)	4.6178(3)	4.5249(1)	4.546(1)
M(1)−As (Å)	3.2063(6)	3.234(2)	3.12680(3)	3.189(7)
M(1)−O (Å) = *a*/2	2.00403(1)	1.99740(5)	2.06149(1)	2.075(1)
M(1) bond distance ratio[a]	1.5999(3)	1.619(1)	1.51677(2)	1.537(3)
M(2)−As (Å)	2.5073	2.426(1)	2.57192(1)	2.577
M(2)−M(2) (Å) = $a/\sqrt{2}$	2.834	2.825	2.918	2.934
As−*M*(2)−As (deg) [2]	106.40	110.80(2)	106.56(3)	107.254

[a]The *M*(1) bond distance ratio given is the *M*(1)−As distance divided by the *M*(1)−O distance.

Since Cr^{2+} with the high spin d^4 configuration is strongly Jahn−Teller active when in an octahedral coordination environment, it is worth making comparison with the crystal structures of other known Sr-containing members of this structural series (Table 5). On comparison with the analogous manganese, iron, and zinc compounds in the series, trends are observed in the size of the lattice parameters which can be explained in terms of the differing ionic radii of the metals.

The most significant comparison is to be made between $Sr_2CrO_2Cr_2As_2$ and the analogous Mn-containing compound $Sr_2MnO_2Mn_2As_2$. Both lattice parameters are significantly shorter in the case of the Cr compound in line with the smaller ionic radius of the d^4 Cr^{2+} ion (0.80 Å)[37] compared with the d^5 Mn^{2+} ion (0.83 Å) with an additional antibonding d electron. The Cr(2)−Cr(2) distance (equal to $a/\sqrt{2}$) across the shared edges of adjacent $CrAs_4$ tetrahedra is 3.4% shorter than the corresponding distance in $Sr_2MnO_2Mn_2As_2$, and the Cr(2)−As distances in the $CrAs_4$ tetrahedra of 2.5073 Å are 2.7% shorter than the corresponding Mn(2)−As distances in $Sr_2MnO_2Mn_2As_2$, although the distortion of the $CrAs_4$ tetrahedron from regular (slight compression along the tetragonal axis) is only marginally larger than in the Mn case. In the oxide layers, the transition metal ion is forced, by the presence of the intervening Sr^{2+} cation, to occupy a highly distended octahedral environment MO_4As_2 with M(1)−As distances that are much larger than in the MAs_4 tetrahedra, reflecting a rather weak interaction between M(1) and As. In $Sr_2CrO_2Cr_2As_2$, the Cr(1)−O distance (equal to $a/2$) is 3.4% shorter than the Mn(1)−O distance in $Sr_2MnO_2Mn_2As_2$, while the long Cr(1)−As distance is 0.5% longer than the corresponding Mn(1)−As distance in $Sr_2MnO_2Mn_2As_2$. The result of accommodating a relatively small ion in the arsenide layer *and* satisfying the coordination requirements of the Sr^{2+} ions results in a CrO_4As_2 coordination environment that is a rather more distended octahedron than that of the corresponding MnO_4As_2 environment. Although d^4 ions such as Cr^{2+} adopt strongly Jahn−Teller distorted octahedral environments in molecules and solids, the ratio of the Cr(1)−As and Cr(1)−O distances of 1.6 in $Sr_2CrO_2Cr_2As_2$ is even larger than the measured Cr−Cl:Cr−O ratio of 1.33 in $Cr(H_2O)_4Cl_2$[38] which is elongated along the Cr−Cl bonds (note that, for comparison, Sr−As ∼ 3.1 Å[39] and Sr−Cl ∼ 3.02 Å[40] distances are fairly similar, so, for the purposes of comparison, we use Cr−Cl distances as a proxy for Cr−As distances), and larger than one would expect based on the ratio of axial and equatorial Cr−Cl distances (4 × 2.39 Å and 2 × 2.90 Å) in the crystal structure of $CrCl_2$.[41] So it is not clear that the increased axial distention around the Cr(1) site in $Sr_2CrO_2Cr_2As_2$ compared with the case in $Sr_2MnO_2Mn_2As_2$ is driven by a Jahn−Teller stabilization. In these compounds, it is probably best to consider the distended $M(1)O_4As_2$ environment as being a consequence of the crystal structure, and this is clear when Sr^{2+} is substituted by Ba^{2+} as the distention becomes very much larger in $Ba_2CrO_2Cr_2As_2$ than could be attributed to a Jahn−Teller distortion (Table 1, Figure 1).

Magnetic Ordering. The observation that the Cr(2) moments in the Cr_2As_2 layer order at a much higher temperature than the Cr(1) moments in the oxide layer is consistent with the observations of Brock et al. for the Mn analogues $Sr_2MnO_2Mn_2As_2$ and $Sr_2MnO_2Mn_2Sb_2$.[3,4] However, while the ordering temperature for the Mn(2) moments in the Mn_2As_2 layer is 340 K in $Sr_2MnO_2Mn_2As_2$, the corresponding Néel temperature (T_{N1}) in the chromium case $Sr_2CrO_2Cr_2As_2$ is 600(10) K. Similarly, the Cr(1) magnetic sublattice of the CrO_2 layers of $Sr_2CrO_2Cr_2As_2$ has a Néel temperature (T_{N2}) estimated as 330(5) K from the PND measurements, whereas in $Sr_2MnO_2Mn_2As_2$ only short-range ordering of the Mn(1) moments in the MnO_2 layer is observed and not until temperatures below 75 K. The considerably higher ordering temperatures in the chromium case are consistent with the observed bond distances. Shorter Cr(2)−Cr(2) and Cr(1)−O distances within the layers, compared with those in the Mn analogue, combined with the less-contracted 3d orbitals of Cr should facilitate stronger intraplanar exchange interactions (via direct Cr(2)−Cr(2) exchange interactions and Cr(2)−As−Cr(2) and Cr(1)−O−Cr(1) superexchange). Indeed, the manganese oxyantimonide of the series, $Sr_2MnO_2Mn_2Sb_2$ with a larger a lattice parameter, has an ordering temperature of the Mn^{2+} ions in the pnictide layer of 300 K, lower than that of the oxyarsenide (340 K). Accordingly, the longer Cr(2)−Cr(2) and Cr(1)−O distances in $Ba_2CrO_2Cr_2As_2$ result in both Cr sublattices undergoing magnetic long-range order at significantly lower temperatures than in $Sr_2CrO_2Cr_2As_2$ (Figure 7).

The other clear differences between $Sr_2CrO_2Cr_2As_2$ and $Ba_2CrO_2Cr_2As_2$ and between these Cr compounds and the Mn analogues lie in the orientations of the moments and in the reorientation transition that is evident in $Sr_2CrO_2Cr_2As_2$ from our work and that of Liu et al.[13] First, we consider the factors that favor particular orientations of moments relative to the crystal axes. The orientation of the magnetic moments of ions in a magnetically ordered array relative to the ligand field may be rationalized on the basis of considerations of spin−orbit coupling as described by Whangbo et al.[42] Because the ligand field does not entirely quench the orbital angular momentum for a 3d transition metal ion, the d orbitals remain associated with their L_z values from the free ion case, if the difference $|\Delta L_z|$ in L_z values between the highest occupied orbital and the lowest unoccupied orbital is 0 then the prediction is that the magnetic moment lies along the z direction where z is the principal axis. If $|\Delta L_z| = 1$, then the moment is predicted to lie perpendicular to the z direction−i.e., in the xy-plane. In the case of $Sr_2CrO_2Cr_2As_2$ and $Ba_2CrO_2Cr_2As_2$, the Cr(1) moments in the oxide layer have highly axially distended octahedral ligand fields (Figure 1) resulting in an orbital arrangement similar to that shown in Figure 10. This leads to

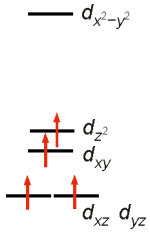

Figure 10. Schematic of the d-orbital splitting in the distended CrO_4As_2 ligand field.

the prediction that the moment will lie along the z direction (i.e., the crystallographic c-axis) according to the argument in Figure 6(a) of ref 42. This is exactly in accord with what we find for the Cr(1) oxide layer moments in $Ba_2CrO_2Cr_2As_2$ from the onset of their ordering at 233 K and for $Sr_2CrO_2Cr_2As_2$ below 247 K after the spin-reorientation

transition is complete. Other experimental cases bear this out. For example, the n = 1 Ruddlesden−Popper-type phase $LaSrMnO_4$[43] contains Mn^{3+} ions with the $3d^4$ configuration in Jahn−Teller-distorted MnO_6 octahedra that have their two longer Mn−O bonds directed along the principal axis of the tetragonal crystal. In this case, which is isoelectronic with the case of $Sr_2CrO_2Cr_2As_2$ and $Ba_2CrO_2Cr_2As_2$, the moments are also found experimentally to lie parallel to the principal axis, in line with the predictions of ref 42.

The corresponding magnetic ions in the oxide layers of $Sr_2MnO_2Mn_2Pn_2$ are Mn^{2+} d^5 moments, and their directional preference is weaker because formally the d^5 configuration carries no orbital angular momentum. Experimentally the Fe^{3+} d^5 moments in $LaSrFeO_4$,[44] $CaPrFeO_4$,[45] and $CaNdFeO_4$[46] are observed to be aligned perpendicular to the crystallographic c-axis at temperatures above the magnetic ordering temperature of the lanthanide moments; and in these cases, the Fe^{3+} ions are in axially distended FeO_6 octahedra ($Fe-O_{ax}/Fe-O_{eq}$ = 1.11 at room temperature), so the ligand fields are qualitatively similar, although less axially distended, to that in $Sr_2MnO_2Mn_2Sb_2$. Thus, the Mn(1) ordered moments in the MnO_2 sheets in $Sr_2MnO_2Mn_2Sb_2$ are oriented in a similar way (within the ab-plane) to analogous antiferromagnetic d^5 systems and perpendicular to the direction which is predicted and found for d^4 Cr^{2+} and Mn^{3+} moments.

Experiments reveal that the Mn^{2+} (d^5) and Cr^{2+} (d^4) moments in LaMnAsO, LaCrAsO, $BaMn_2As_2$, and $BaCr_2As_2$[30] all undergo antiferromagnetic ordering with their Mn or Cr moments aligned parallel to the c-axis. This is also the experimentally observed orientation of the moments corresponding to the Mn(2) (d^5) or Cr(2) (d^4) ions in $Sr_2MnO_2Mn_2Pn_2$ and $Ba_2CrO_2Cr_2As_2$ (at all temperatures) or $Sr_2CrO_2Cr_2As_2$ (at temperatures above the ordering temperature of the Cr(1) moments). So, we conclude that these are the preferred moment orientations for these tetrahedral moments. Thus, in $Ba_2CrO_2Cr_2As_2$ and $Sr_2MnO_2Mn_2Sb_2$ where there is long-range magnetic order on both transition metal sublattices, the preferred moment directions on both sublattices are found experimentally below the respective ordering temperatures.

Like $Ba_2CrO_2Cr_2As_2$, but in contrast to the $Sr_2MnO_2Mn_2Pn_2$ cases, $Sr_2CrO_2Cr_2As_2$ contains two sublattices of Cr^{2+} moments which both have a preference, for alignment along the c-axis. In all these compounds, the two different transition metal moments order with different propagation vectors (k = (1 1 1) for the Cr(2) (or Mn(2)) moments in the pnictide layers and k = (1/2 1/2 0) for the Cr(1) (or Mn(1)) moments in the oxide layers. There should thus be no direct coupling between the Cr(1) and Cr(2) sublattices. However, we (and Liu et al.[13]) observe that in $Sr_2CrO_2Cr_2As_2$ ordering of the Cr(1) moments in the oxide layer drives a spin-reorientation transition as the magnitude of the ordered Cr(1) moment increases (Figures 6(a) and 7(b)) with the moments on the two sublattices remaining orthogonal. Thus, the sublattices must communicate, and there is a preference for the moments to be orthogonal (see below). We propose that the preference for alignment parallel to c is stronger for the Cr(1) ions in the oxide layer than it is for the Cr(2) moments in the arsenide layer, presumably due to the greater anisotropy of the ligand field, and this presumably accounts for the magnetic ground state. The spin-reorientation transition in $Sr_2CrO_2Cr_2As_2$ bears some qualitative resemblance to the spin-reorientations driven by the ordering of lanthanide moments in compounds containing MnPn layers (e.g., the CeMnAsO,[20,53] NdMnAsO,[18,19] and PrMnSbO,[47] members of the LnMnAsO series) and layered perovskite-related compounds containing ordered arrays of transition metal moments (e.g., $CaNdFeO_4$[46] and $CaPrFeO_4$[45]), but in these cases, direct coupling of the transition metal and lanthanide magnetic sublattices is permitted because they order with the same propagation vector.

While powder neutron diffraction measurements place an intrinsic constraint on knowing the moment orientation in an ordered system,[35] we note that for the tetragonal system, the moment component along the principal c-axis may be determined unambiguously, while the orientation of any component within the ab-plane perpendicular to the principal axis is uncertain. In $Sr_2CrO_2Cr_2As_2$ with one moment parallel to c and one moment perpendicular to c, it is clear that the Cr(1) and Cr(2) moments are orthogonal. Thus, exchange interactions that rely on scalar products of the spins of these two sublattices (e.g., Heisenberg symmetric exchange or biquadratic exchange) will be zero, while terms that are vector products of the spins (Dzyaloshinskii-Moriya (DM) antisymmetric exchange) will be nonzero. A DM interaction between the orthogonal Cr(1) and Cr(2) moments could, in principle, be responsible for maintaining their orthogonality. The strength of the DM interaction depends on the size of the spins, on the spin−orbit coupling constant of the Cr^{2+} ions, and on the size of the unquenched orbital moment of the ions.[48] In this case, the d^4 Cr(2) ion in a slightly distorted tetrahedral environment is expected to carry a significant orbital moment and would result in a significant DM interaction.

For the DM interaction to provide this orthogonality, however, requires the two sublattices to couple. The group theoretical analysis presented in the Supporting Information (Figure S6 and Figure S7 plus accompanying description) describes a likely structural distortion with tilting of the CrO_2 sheets and in-plane antipolar displacements of the Sr and As atoms. However, high resolution diffraction data from I11 at temperatures below and across the spin-reorientation transition gave no evidence for such a distortion: the refinements were not unstable, but there was no clear improvement to the fit, and the displacements of atoms from their ideal positions (i.e., those of the $I4/mmm$ structure) were a factor of 10−100 smaller than the uncertainties in the refined parameters.

We probed $Sr_2CrO_2Cr_2As_2$ further using electron microscopy. Room temperature electron diffraction (ED) patterns taken along the main crystallographic directions on different crystallites agree with the $I4/mmm$ space group (Figure 11(a)−(c)). No additional extinction conditions were evident in these patterns that suggested a symmetry lowering, nor were any changes evident on cooling to ∼100 K (∼−170 °C), well below the spin-reorientation transition. HAADF-STEM experiments did reveal further structural features of $Sr_2CrO_2Cr_2As_2$ which were not evident from the bulk diffraction measurements. The HAADF-STEM images in Figure 12(a) show well-ordered regions, consistent with the sharp ED patterns in Figure 11(a)−(c); however, diffuse streaks were observed on some ED patterns acquired along the [100] direction (Figure 11(d)) suggesting large concentrations of stacking faults. The faults are characterized by the relative translation (by $a/2$) of the two planes of arsenide ions that form the CrAs layers (close-up in the HAADF-STEM image of a faulted region in Figure 12(b)). Figure 12(b) shows that these stacking faults

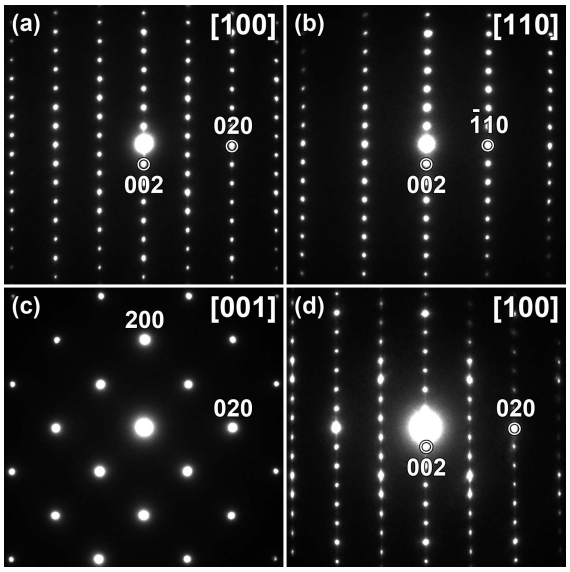

Figure 11. Representative ED patterns taken along the main directions: [100] (a), [110] (b), and [001] (c). The majority of crystals probed produced diffraction patterns as in (a)−(c), corresponding to the well ordered structure for which the HAADF-STEM image is shown along [100] in Figure 12(a). The [100] ED pattern in (d) shows the presence of diffuse streaks along 0*k*0 lines as a consequence of the stacking faults found in some of the crystallites (Figure 12(b)).

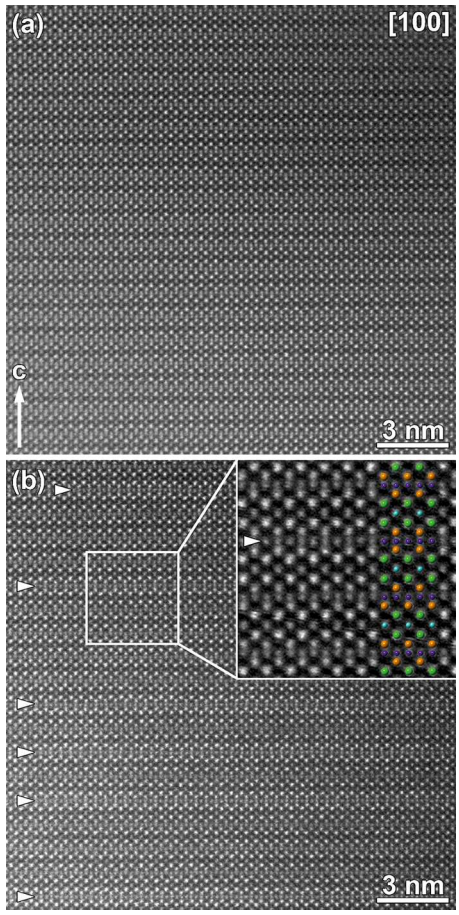

Figure 12. HAADF-STEM images taken from a well-ordered crystal (a) and a crystal with stacking faults (b). The atom identities are inserted on the enlarged image in (b) (Sr−green; As−orange; Cr1−turquoise; Cr2−violet; oxygen atoms are not shown for clarity). The randomly distributed stacking faults are indicated with arrowheads. See also Figure S9 and Figure S10.

can occur in quite high concentrations and a random manner. Occasionally, the stacking faults show long-range order, resulting in additional reflections in the ED patterns (Figure S10). It is possible that these faults arise from slight oxidation of part of the sample with the conversion of a Cr_2As_2 layer to a Cr_2OAs_2 layer containing Cr_2O sheets similar to those found for other transition metals, notably Fe, in numerous compounds: $La_2Fe_2Se_2O_3$[49] and relatives such as $Sr_2Fe_2Se_2OF_2$,[50] $Na_2Fe_2Se_2O$,[51] and $BaFe_2Se_2O$.[52] This oxidation to produce Cr^{3+} ions in these layers is consistent with the facile oxidation of Cr^{2+}. However, further investigation is required on this point. The electron microscopy measurements also identified a well-crystallized minority phase which was more oxide rich and has the formula Sr_2CrO_3CrAs, isostructural with Sr_2MnO_3CuS,[36] with thicker oxide layers separating the CrAs layers. Adding this phase to the Rietveld refinements at the 1.3(1)% level by mass accounted for weak reflections that could not be accounted for by other impurities (see Figure 1, Figure 8). We have subsequently been able to synthesize this phase in the bulk form, and its characterization will be reported elsewhere.

Neither the electron microscopy measurements nor the high resolution synchrotron X-ray diffraction measurements provide evidence for a symmetry-lowering distortion that would allow the two magnetic sublattices to couple and enable the DM interaction to stabilize the orthogonal moments. Nevertheless, the experimental observation by us and by Liu et al.[13] for $Sr_2CrO_2Cr_2As_2$ is that the ordering of the Cr(1) moments precipitates a spin reorientation of the already-ordered Cr(2) moments and the Cr(1) and Cr(2) moments maintain orthogonality, and this must be enabled by some other mechanism.

In CeMnAsO[20] where there is also a spin-reorientation transition, the behavior of the magnetic reflections suggested an orthorhombic distortion at low temperature in data collected using a fairly high resolution neutron powder neutron diffractometer (OSIRIS at ISIS[20]), but in that case, we went on to show that no symmetry-lowering distortion was observed in the low temperature powder X-ray diffraction, collected at much higher resolution using the synchrotron beamline ID31 at ESRF, although there was a decrease in the *c*/*a* ratio at the spin-reorientation transition in CeMnAsO (also noted by Zhang et al.[53] We proposed that a very small incommensurability of the magnetic and nuclear structures could account for the behavior of CeMnAsO.[20] The behavior at the spin reorientation transition in $Sr_2CrO_2Cr_2As_2$ seems similar to that in CeMnAsO; so, a possible conclusion that would account for the spin reorientation is that the long-range magnetic ordering has a small incommensurability with the underlying crystal structure, and our assumption that the Cr(2) moments order with a propagation vector k = (1 1 1) and the Cr(1) moments order with a propagation vector k = (1/2 1/2 0) is an oversimplification. The experimental support for this incommensurability is the observation of shifts in magnetic Bragg peaks (see Figure 9) suggestive of a symmetry-lowering distortion, despite the lack of evidence for this in the crystal structure and by the appearance of the additional scattering observed at about d = 16.5 Å in the neutron diffractogram (Figure 8). Attempts to model the behavior of the magnetic

scattering using a more sophisticated model were not successful—the small relative shifts of the positions of the magnetic peaks in Figure 9 suggest that the incommensurate solution is a spin density wave with a propagation vector of (0.4995 0.5003 0), but attempted refinements set this back to the commensurate value of (1/2 1/2 0). $Ba_2CrO_2Cr_2As_2$, where there is no spin-reorientation transition, shows no evidence that its magnetic structure is incommensurate. The reason why $Ba_2CrO_2Cr_2As_2$ differs from the Sr analogue is unclear. The only significant structural difference between them is the much larger Cr(1)—As distance in $Ba_2CrO_2Cr_2As_2$, meaning that the $Cr(1)O_4As_2$ octahedron is much more distended in $Ba_2CrO_2Cr_2As_2$ compared with $Sr_2CrO_2Cr_2As_2$. It is not clear how this relates to the anomalous behavior of $Sr_2CrO_2Cr_2As_2$, although it would presumably be a key factor in determining the strength of Cr(1)—Cr(2) coupling. We suggest that further insight into the spin-reorientation transition of $Sr_2CrO_2Cr_2As_2$ may be obtained in a single crystal neutron diffraction investigation supported by high level computation. Whether the faulting observed in some grains of the sample in the electron diffraction and STEM images is relevant to the magnetic behavior or is unrelated to it also requires further investigation, but at least it underlines the structural complexity of these intergrowth phases. We note that $Sr_2Mn_{2.23}Cr_{0.77}As_2O_2$, a member of the solid solution between all-Mn and all-Cr end members, has recently been reported, and this also shows a complex series of magnetic transitions and spin reorientations.[54]

■ ASSOCIATED CONTENT

Supporting Information

The Supporting Information is available free of charge at https://pubs.acs.org/doi/10.1021/acs.inorgchem.0c02415.

Tables of refined parameters, analysis of variable temperature diffraction data, further Rietveld refinement results, magnetic symmetry analysis of spin reorientation, further electron microscopy results, and magnetometry data (PDF)

■ AUTHOR INFORMATION

Corresponding Author

Simon J. Clarke — *Inorganic Chemistry Laboratory, Department of Chemistry, University of Oxford, Oxford OX1 3QR, U.K.;* orcid.org/0000-0003-4599-8874; Email: simon.clarke@chem.ox.ac.uk

Authors

Xiaoyu Xu — *Inorganic Chemistry Laboratory, Department of Chemistry, University of Oxford, Oxford OX1 3QR, U.K.*

Michael A. Jones — *Inorganic Chemistry Laboratory, Department of Chemistry, University of Oxford, Oxford OX1 3QR, U.K.*

Simon J. Cassidy — *Inorganic Chemistry Laboratory, Department of Chemistry, University of Oxford, Oxford OX1 3QR, U.K.*

Pascal Manuel — *ISIS Facility, STFC Rutherford Appleton Laboratory, Harwell Oxford, Didcot OX11 0QX, United Kingdom*

Fabio Orlandi — *ISIS Facility, STFC Rutherford Appleton Laboratory, Harwell Oxford, Didcot OX11 0QX, United Kingdom;* orcid.org/0000-0001-6333-521X

Maria Batuk — *Electron Microscopy for Materials Science (EMAT), University of Antwerp, B-2020 Antwerp, Belgium;* orcid.org/0000-0003-1411-9785

Joke Hadermann — *Electron Microscopy for Materials Science (EMAT), University of Antwerp, B-2020 Antwerp, Belgium;* orcid.org/0000-0002-1756-2566

Author Contributions

X.X. and M.A.J. synthesized the samples and with S.J.C. collected and analyzed the diffraction and magnetometry data. M.B. and J.H. collected and analyzed the electron diffraction and microscopy data. F.O. and P.M. provided technical support on WISH and analyzed the spin-reorientation. S.J.C. wrote the paper with input from the other authors.

Notes

The authors declare no competing financial interest.

■ ACKNOWLEDGMENTS

We thank the UK EPSRC (EP/M020517/1 and EP/P018874/1) and the Leverhulme Trust (RPG-2014-221) for funding and the ISIS pulsed neutron and muon source (RB1610357 and RB1700075) and the Diamond Light Source Ltd. (EE13284 and EE18786) for the award of beam time. We thank Dr. A. Baker and Dr. C. Murray for support on I11.

■ REFERENCES

(1) Brechtel, E.; Cordier, G.; Schäfer, H. Über Oxidpnictide: Zur Kenntnis von $A_2Mn_3B_2O_2$ mit A = Sr, Ba und B = As, Sb, Bi/On Oxidpnictides: Preparation and Crystal Structure of $A_2Mn_3B_2O_2$ with A = Sr, Ba and B = As, Sb, Bi. *Z. Naturforsch., B: J. Chem. Sci.* **1979**, *34*, 777—780.

(2) Stetson, N. T.; Kauzlarich, S. M. A new material with alternating metal-oxide and metal-phosphide layers: barium manganese phosphate ($Ba_2Mn_3P_2O_2$). *Inorg. Chem.* **1991**, *30*, 3969—3971.

(3) Brock, S. L.; Raju, N.; Greedan, J.; Kauzlarich, S. M. The magnetic structures of the mixed layer pnictide oxide compounds $Sr_2Mn_3Pn_2O_2$ (Pn = As, Sb). *J. Alloys Compd.* **1996**, *237*, 9—19.

(4) Brock, S. L.; Kauzlarich, S. M. Structure-property relationships in a series of mixed layer pnictide oxide compounds: $A_2Mn_3Pn_2O_2$ (A Sr, Ba; PnP, As, Sb). *J. Alloys Compd.* **1996**, *241*, 82—88.

(5) Pöttgen, R.; Johrendt, D. Materials with ZrCuSiAs-type Structure. *Z. Naturforsch., B: J. Chem. Sci.* **2008**, *63*, 1135—1148.

(6) Muir, S.; Subramanian, M. A. ZrCuSiAs type layered oxypnictides: A bird's eye view of LnMPnO compositions. *Prog. Solid State Chem.* **2012**, *40*, 41—56.

(7) Just, G.; Paufler, P. On the coordination of $ThCr_2Si_2$ ($BaAl_4$)-type compounds within the field of free parameters. *J. Alloys Compd.* **1996**, *232*, 1—25.

(8) Belsky, A.; Hellenbrandt, M.; Karen, V. L.; Luksch, P. New developments in the Inorganic Crystal Structure Database (ICSD): accessibility in support of materials research and design. *Acta Crystallogr., Sect. B: Struct. Sci.* **2002**, *58*, 364—369.

(9) Brock, S. L.; Kauzlarich, S. M. $A_2Zn_3As_2O_2$ (A = Ba, Sr): A Rare Example of Square Planar Zinc. *Inorg. Chem.* **1994**, *33*, 2491—2492.

(10) Ozawa, T.; Olmstead, M. M.; Brock, S. L.; Kauzlarich, S. M.; Young, D. M. Synthesis and Characterization of a New Compound with Alternating MnO_2^{2-} and $Zn_2As_2^{2-}$ Layers: $Ba_2MnZn_2As_2O_2$. *Chem. Mater.* **1998**, *10*, 392—396.

(11) Ozawa, T. C.; Kauzlarich, S. M.; Bieringer, M.; Wiebe, C. R.; Greedan, J. E.; Gardner, J. S. The Effect of Interlayer Cations on the Magnetic Properties of the Mixed-Metal Pnictide Oxides: $A_2MnZn_2As_2O_2$ (A = Sr, Ba). *Chem. Mater.* **2001**, *13*, 973—980.

(12) Jiang, H.; Bao, J.-K.; Zhai, H.-F.; Tang, Z.-T.; Sun, Y.-L.; Liu, Y.; Wang, Z.-C.; Bai, Z.-C.; Xu, Z.-A.; Cao, G.-H. Physical properties and electronic structure of $Sr_2Cr_3As_2O_2$ containing CrO_2 and Cr_2As_2 square-planar lattices. *Phys. Rev. B: Condens. Matter Mater. Phys.* **2015**, *92*, 205107.
(13) Liu, J.; Wang, J.; Sheng, J.; Ye, F.; Taddei, K. M.; Fernandez-Baca, J. A.; Luo, W.; Sun, G.-A.; Wang, Z.-C.; Jiang, H.; Cao, G.-H.; Bao, W. Neutron diffraction study on magnetic structures and transitions in $Sr_2Cr_3As_2O_2$. *Phys. Rev. B: Condens. Matter Mater. Phys.* **2018**, *98*, 134416.
(14) Ozawa, T. C.; Kauzlarich, S. M. Chemistry of layered d-metal pnictide oxides and their potential as candidates for new superconductors. *Sci. Technol. Adv. Mater.* **2008**, *9*, 033003.
(15) Clarke, S. J.; Adamson, P.; Herkelrath, S. J. C.; Rutt, O. J.; Parker, D. R.; Pitcher, M. J.; Smura, C. F. Structures, Physical Properties, and Chemistry of Layered Oxychalcogenides and Oxypnictides. *Inorg. Chem.* **2008**, *47*, 8473−8486.
(16) Hayward, M. A. Synthesis and Magnetism of Extended Solids Containing Transition-Metal Cations in Square-Planar, MO_4 Coordination Sites. *Inorg. Chem.* **2019**, *58*, 11961−11970.
(17) Singh, Y.; Green, M. A.; Huang, Q.; Kreyssig, A.; McQueeney, R. J.; Johnston, D. C.; Goldman, A. I. Magnetic order in $BaMn_2As_2$ from neutron diffraction measurements. *Phys. Rev. B: Condens. Matter Mater. Phys.* **2009**, *80*, 100403R.
(18) Emery, N.; Wildman, E. J.; Skakle, J. M. S.; Mclaughlin, A. C.; Smith, R. I.; Fitch, A. N. Variable temperature study of the crystal and magnetic structures of the giant magnetoresistant materials LMnAsO-(L = La, Nd). *Phys. Rev. B: Condens. Matter Mater. Phys.* **2011**, *83*, 144429.
(19) Marcinkova, A.; Hansen, T. C.; Curfs, C.; Margadonna, S.; Bos, J. W. G. Nd-induced Mn spin-reorientation transition in NdMnAsO. *Phys. Rev. B: Condens. Matter Mater. Phys.* **2010**, *82*, 174438.
(20) Corkett, A. J.; Free, D. G.; Clarke, S. J. Spin-Reorientation Transition in CeMnAsO. *Inorg. Chem.* **2015**, *54*, 1178−1184.
(21) Enjalran, M.; Scalettar, R. T.; Kauzlarich, S. M. Magnetic states in frustrated bilayer models: The ordered phase of mixed-layer pnictide oxides. *Phys. Rev. B: Condens. Matter Mater. Phys.* **2000**, *61*, 14570−14580.
(22) Nath, R.; Garlea, V. O.; Goldman, A. I.; Johnston, D. C. Synthesis, structure, and properties of tetragonal $Sr_2M_3As_2O_2$ (M_3 = Mn_3, Mn_2Cu, and $MnZn_2$) compounds containing alternating CuO_2-type and FeAs-type layers. *Phys. Rev. B: Condens. Matter Mater. Phys.* **2010**, *81*, 224513.
(23) An, J.; Sefat, A. S.; Singh, D. J.; Du, M.-H. Electronic structure and magnetism in $BaMn_2As_2$ and $BaMn_2Sb_2$. *Phys. Rev. B: Condens. Matter Mater. Phys.* **2009**, *79*, 075120.
(24) Singh, Y.; Ellern, A.; Johnston, D. C. Magnetic, transport, and thermal properties of single crystals of the layered arsenide $BaMn_2As_2$. *Phys. Rev. B: Condens. Matter Mater. Phys.* **2009**, *79*, 094519.
(25) Tsukamoto, Y.; Okamoto, Y.; Matsuhira, K.; Whangbo, M.-H.; Hiroi, Z. A Magnetic Transition Probed by the Ce Ion in Square-Lattice Antiferromagnet CeMnAsO. *J. Phys. Soc. Jpn.* **2011**, *80*, 094708.
(26) Eguchi, N.; Ishikawa, F.; Kodama, M.; Wakabayashi, T.; Nakayama, A.; Ohmura, A.; Yamada, Y. Synthesis of New Layered Oxypnictides $Sr_2CrO_2(FeAs)_2$. *J. Phys. Soc. Jpn.* **2013**, *82*, 045002.
(27) Yuzuri, M. On the Magnetic Properties of Cr_2As and Cu_2Sb. *J. Phys. Soc. Jpn.* **1960**, *15*, 2007.
(28) Park, S.-W.; Mizoguchi, H.; Kodama, K.; Shamoto, S.; Otomo, T.; Matsuishi, S.; Kamiya, T.; Hosono, H. Magnetic Structure and Electromagnetic Properties of LnCrAsO with a ZrCuSiAs-type Structure (Ln = La, Ce, Pr, and Nd). *Inorg. Chem.* **2013**, *52*, 13363−13368.
(29) Singh, D. J.; Sefat, A. S.; McGuire, M. A.; Sales, B. C.; Mandrus, D.; VanBebber, L. H.; Keppens, V. Itinerant antiferromagnetism in $BaCr_2As_2$: Experimental characterization and electronic structure calculations. *Phys. Rev. B: Condens. Matter Mater. Phys.* **2009**, *79*, 094429.
(30) Filsinger, K. A.; Schnelle, W.; Adler, P.; Fecher, G. H.; Reehuis, M.; Hoser, A.; Hoffmann, J.-U.; Werner, P.; Greenblatt, M.; Felser, C. Antiferromagnetic structure and electronic properties of $BaCr_2As_2$ and $BaCrFeAs_2$. *Phys. Rev. B: Condens. Matter Mater. Phys.* **2017**, *95*, 184414.
(31) Thompson, S. P.; Parker, J. E.; Potter, J.; Hill, T. P.; Birt, A.; Cobb, T. M.; Yuan, F.; Tang, C. C. *Rev. Sci. Instrum.* **2009**, *80*, 075107.
(32) Chapon, L. C.; Manuel, P.; Radaelli, P. G.; Benson, C.; Perrott, L.; Ansell, S.; Rhodes, N. J.; Raspino, D.; Duxbury, D.; Spill, E.; Norris, J. WISH: The New Powder and Single Crystal Magnetic Diffractometer on the Second Target Station. *Neutron News* **2011**, *22*, 22−25.
(33) Coelho, A. A. *TOPAS academic: General profile and Structure Analysis Software For Powder Diffraction Data*; Bruker AXS: Karlsruhe, Germany, 2012.
(34) Campbell, B. J.; Stokes, H. T.; Tanner, D. E.; Hatch, D. M. ISODISPLACE: a web-based tool for exploring structural distortions. *J. Appl. Crystallogr.* **2006**, *39*, 607−614.
(35) Shirane, G. A note on the magnetic intensities of powder neutron diffraction. *Acta Crystallogr.* **1959**, *12*, 282−285.
(36) Zhu, W. J.; Hor, P. H. Synthesis and Structure of Layered Manganese Oxychalcogenides: Sr_2CuMnO_3S and $Sr_4Cu_2Mn_3O_{7.5}Q_2$ (Q = S, Se). *J. Solid State Chem.* **2000**, *153*, 26−29.
(37) Shannon, R. D. *Acta Crystallogr., Sect. A: Cryst. Phys., Diffr., Theor. Gen. Crystallogr.* **1976**, *A32*, 751−767.
(38) von Schnering, H. G.; Brand, B.-H. Struktur und Eigenschaften des blauen Chrom(II)-chlorid-tetrahydrats $CrCl_2 \cdot 4H_2O$. *Z. Anorg. Allg. Chem.* **1973**, *402*, 159−168.
(39) Somer, M.; Carrillo Cabrera, W.; Peters, K.; von Schnering, H. G. Crystal structure of tetrastrontium triarsenide, Sr_4As_3. *Z. Kristallogr. - Cryst. Mater.* **1995**, *210*, 876−876.
(40) Brauer, G.; Müller, O. Zur Kristallchemie des Strontium-chlorids. *Z. Anorg. Allg. Chem.* **1958**, *295*, 218−226.
(41) Howard, C. J.; Kennedy, B. J.; Curfs, C. Temperature-induced structural changes in $CaCl_2$,$CaBr_2$, and $CrCl_2$: A synchrotron x-ray powder diffraction study. *Phys. Rev. B: Condens. Matter Mater. Phys.* **2005**, *72*, 214114.
(42) Whangbo, M.-H.; Gordon, E. E.; Xiang, H.; Koo, H.-J.; Lee, C. Prediction of Spin Orientations in Terms of HOMO−LUMO Interactions Using Spin−Orbit Coupling as Perturbation. *Acc. Chem. Res.* **2015**, *48*, 3080−3087.
(43) Senff, D.; Reutler, P.; Braden, M.; Friedt, O.; Bruns, D.; Cousson, A.; Bourée, F.; Merz, M.; Büchner, B.; Revcolevschi, A. Crystal and magnetic structure of $La_{1-x}Sr_{1+x}MnO_4$: Role of the orbital degree of freedom. *Phys. Rev. B: Condens. Matter Mater. Phys.* **2005**, *71*, 024425.
(44) Qureshi, N.; Ulbrich, H.; Sidis, Y.; Cousson, A.; Braden, M. Magnetic structure and magnon dispersion in $LaSrFeO_4$. *Phys. Rev. B: Condens. Matter Mater. Phys.* **2013**, *87*, 054433.
(45) Qureshi, N.; Valldor, M.; Weber, L.; Senyshyn, A.; Sidis, Y.; Braden, M. Magnetic spin-flop transition and interlayer spin-wave dispersion in $PrCaFeO_4$ revealed by neutron diffraction and inelastic neutron scattering. *Phys. Rev. B: Condens. Matter Mater. Phys.* **2015**, *91*, 224402.
(46) Oyama, S.; Wakeshima, M.; Hinatsu, Y.; Ohoyama, K. Spin reorientation transition in layered perovskite $CaNdFeO_4$. *J. Phys.: Condens. Matter* **2004**, *16*, 8429−8446.
(47) Kimber, S. A. J.; Hill, A. H.; Zhang, Y.-Z.; Jeschke, H. O.; Valentí, R.; Ritter, C.; Schellenberg, I.; Hermes, W.; Pöttgen, R.; Argyriou, D. N. Local moments and symmetry breaking in metallic PrMnSbO. *Phys. Rev. B: Condens. Matter Mater. Phys.* **2010**, *82*, 100412R.
(48) Dai, D.; Xiang, H.; Whangbo, M.-H. Effects of Spin-Orbit Coupling on Magnetic Properties of Discrete and Extended Magnetic Systems. *J. Comput. Chem.* **2008**, *29*, 2187−2209.
(49) Mayer, J. M.; Schneemeyer, L. F.; Siegrist, T.; Waszczak, J. V.; Van Dover, B. New Layered Iron-Lanthanum-Oxide-Sulfide and

-Selenide Phases: $Fe_2La_2O_3E_2$ (E= S,Se). *Angew. Chem., Int. Ed. Engl.* **1992**, *31*, 1645−1647.
(50) Kabbour, H.; Janod, E.; Corraze, B.; Danot, M.; Lee, C.; Whangbo, M.-H.; Cario, L. Structure and Magnetic Properties of Oxychalcogenides $A_2F_2Fe_2OQ_2$ (A = Sr, Ba; Q = S, Se) with Fe_2O Square Planar Layers Representing an Antiferromagnetic Checkerboard Spin Lattice. *J. Am. Chem. Soc.* **2008**, *130*, 8261−8270.
(51) He, J. B.; Wang, D. M.; Shi, H. L.; Yang, H. X.; Li, J. Q.; Chen, G. F. Synthesis, structure, and magnetic properties of the layered iron oxychalcogenide $Na_2Fe_2Se_2O$. *Phys. Rev. B: Condens. Matter Mater. Phys.* **2011**, *84*, 205212.
(52) Takeiri, F.; Matsumoto, Y.; Yamamoto, T.; Hayashi, N.; Li, Z.; Tohyama, T.; Tassel, C.; Ritter, C.; Narumi, Y.; Hagiwara, M.; Kageyama, H. High-pressure synthesis of the layered iron oxyselenide $BaFe_2Se_2O$ with strong magnetic anisotropy. *Phys. Rev. B: Condens. Matter Mater. Phys.* **2016**, *94*, 184426.
(53) Zhang, Q.; Kumar, C. M. N.; Tian, W.; Dennis, K. W.; Goldman, A. I.; Vaknin, D. Structure and magnetic properties of *Ln*MnSbO (*Ln* = La and Ce). *Phys. Rev. B: Condens. Matter Mater. Phys.* **2016**, *93*, 094413.
(54) Lawrence, G. B.; Wildman, E. J.; Stenning, G. B. G.; Ritter, C.; Fauth, F.; Mclaughlin, A. C. Electronic and Magnetic Properties of Cation Ordered $Sr_2Mn_{2.23}Cr_{0.77}As_2O_2$. *Inorg. Chem.* **2020**, *59*, 7553−7560.